ACS OMEGA

http://pubs.acs.org/journal/acsodf

Article

Photo-oxidative Decolorization of Brilliant Blue with AgNPs as an Activator in the Presence of $K_2S_2O_8$ and $NaBH_4$

Abeer Saad Al-Shehri, Zoya Zaheer,* Amell Musaid Alsudairi, and Samia A. Kosa

Cite This: *ACS Omega* 2021, 6, 27510−27526

Read Online

ACCESS | Metrics & More | Article Recommendations

ABSTRACT: The decolorization of brilliant blue (E133) in aqueous solution by $K_2S_2O_8$ and $NaBH_4$ with AgNPs as an activator was studied spectrophotometrically under normal laboratory conditions. Batch experiments were performed to investigate the effects of reaction time, initial dye concentration, activator concentration, solution pH, and temperature on the decolorization of E133. $K_2S_2O_8$ and $NaBH_4$ did not decolorize the dye E133 in the absence of AgNPs. The optimum dosage of AgNPs was 0.01 g/L, and 98% dye E133 degradation was observed with 3.75 mM $K_2S_2O_8$ at 30 °C in ca. 60 min of reaction time. In the $NaBH_4$/AgNPs system, only 60% dye degradation was observed for an identical reaction condition. The decolorization rate constant increases with the increase in concentrations of AgNPs, $K_2S_2O_8$, $NaBH_4$, and reaction temperature. The decolorization degree of the E133 responded linearly with $K_2S_2O_8$ and $NaBH_4$ concentrations. The existence of sulfate radicals ($SO_4^{\cdot-}$) and hydroxyl radicals ($HO^{\cdot}$) generated during the decolorization of E133 was identified by using ethanol and tertiary butyl alcohol as scavengers. Based on the E133 solution absorbance changes at 628 nm, the decolorization mechanism was proposed and discussed.

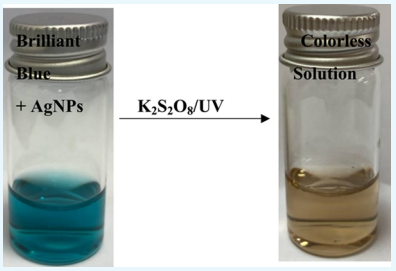

INTRODUCTION

Triphenylmethane dyes are extensively used in various industries such as cosmetic, food, leather, paper, and textile for many purposes from many decades.[1−5] The expanding use of triphenylmethane dyes in textile industries for dying cotton, nylon, and wool may cause substantial ecological damage due to the release of different dyes into the environment.[6] Brilliant blue FCF is a water-soluble triphenylmethane dye, generally used as a water tracer agent.[7] Due to its nontoxic activities, brilliant blue has been used as a food colorant as well as to stain cell bacterial and fungal cells.[8,9] Weber et al. reported that brilliant blue shows an allergic reaction in some bronchial asthma patients.[10] The photocytotoxicity of triphenylmethane dye depends on the production of reactive oxygen species with regard to their photodynamic therapy.[11] The use of dyes as a food coloring agent has serious impact on human health and environment.[12]

Scheme 1. Structure of Brilliant Blue (Blue 1)

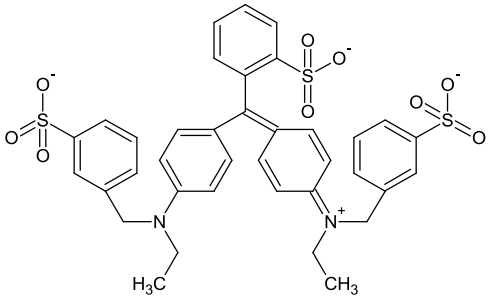

Advanced oxidation technologies (AOTs) have been considered as important technologies for accelerating the oxidation and/or decolorization of a wide range of organic contaminants from polluted wastewater and air.[13] AOTs were based on *in situ* generation of highly reactive oxidizing radicals, such as $HO^{\cdot}$ and $SO_4^{\cdot-}$, to oxidize organic pollutants using common oxidants such as hydrogen peroxide,[14] Fenton's reagent,[15] potassium persulfate,[16] potassium periodate,[17] and potassium bromate.[18] Out of these, potassium persulfate will get an edge over the other oxidants due to its nonselective reactivity, stability, high aqueous solubility, ease of storage, relatively low cost, and higher reduction potential (E_0 of $S_2O_8^{2-}/SO_4^{2-}$ = 2.01 V) in aqueous solution at neutral pH. Berlin[19] and Huag et al.[20] reported the generation of $HO^{\cdot}$ (E_0 = 2.8 V) and $SO_4^{\cdot-}$ (E_0 = 2.6 V) during the thermal decomposition of $S_2O_8^{2-}$ ions in an aqueous phase. These radicals were also generated by the activation of $S_2O_8^{2-}$ ions by UV irradiation,[21] transition metals,[22] and metal nanoparticles.[23]

Received: August 18, 2021
Accepted: September 28, 2021
Published: October 8, 2021

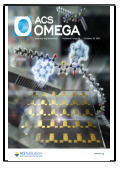

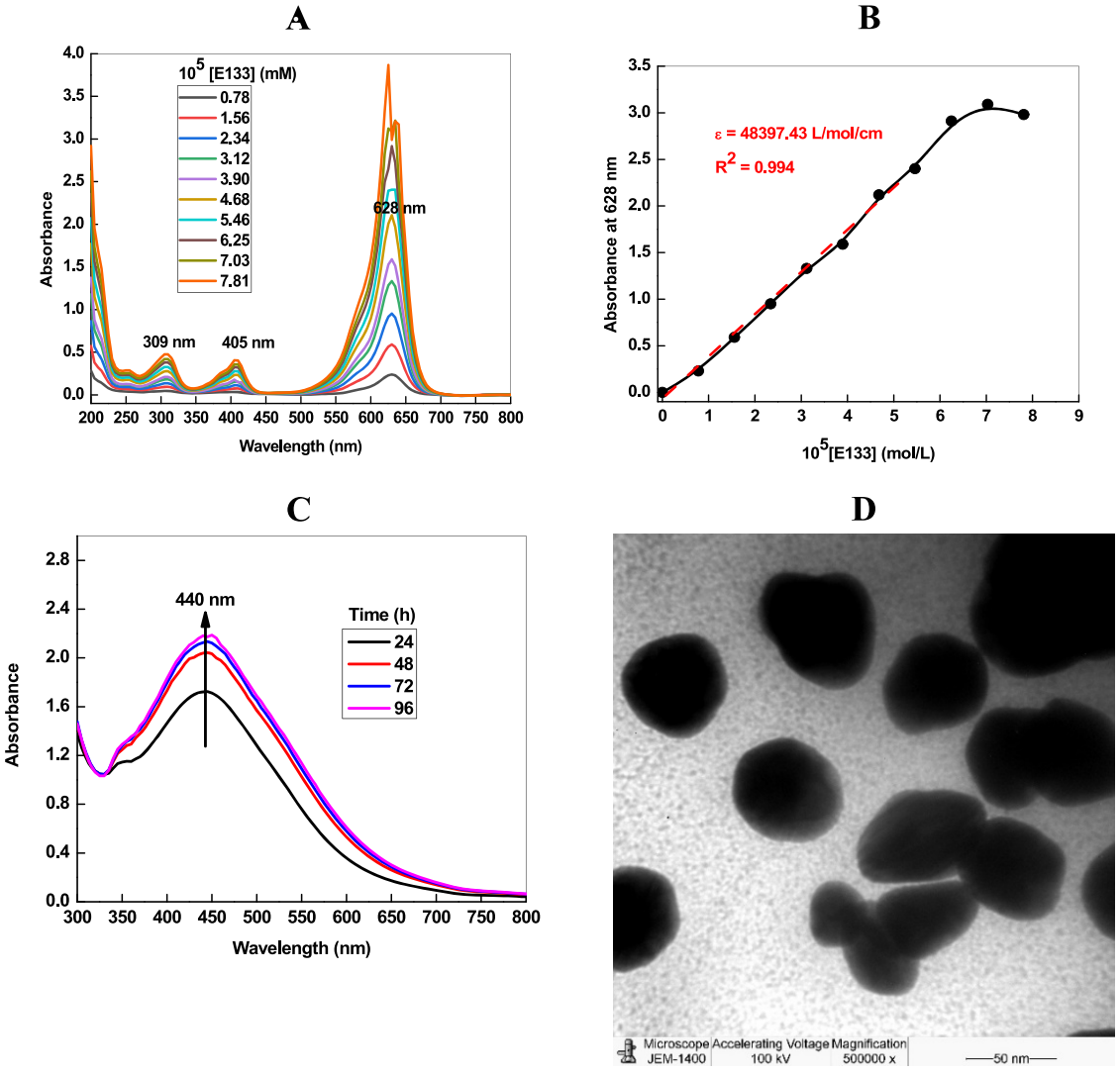

Figure 1. UV−visible spectra of E133 as a function of different concentrations (A), Beer−Lambert plot (B), UV−visible spectra of AgNPs (C), and its TEM image (D) at 30 °C. Reaction conditions: [$AgNO_3$] = 1.25 mM, [hydrazine] = 5.0 mM, and [CTAB] = 0.8 mM for C.

Sodium borohydride is a better source of hydrogen and is generally used as a reducing agent (E_0 = 1.24 V) for the synthesis of advanced transition metal nanoparticles. It is also used as a source of hydrogen to the reduction of metal ions and oxidative discoloration of various toxic nonbiodegradable organic dyes and other compounds in the presence of metal NPs.[24−26] The surface of NPs plays a significant role (electron relay effect) during the transfer of hydrogen from $NaBH_4$ to the oxidizing agent. For example, Kaur and her co-workers reported the extraction of gold and silver nanoparticles from the aqueous phase by using water-soluble iron oxide nanoparticles and suggested that the degree of extraction depends on the strength of interactions between the AuNPs and AgNPs with Fe_2O_3 NPs.[27] Pal and his co-workers reported the degradation of aromatic nitro phenols by using AgNPs as a catalyst in the presence of $NaBH_4$.[28] Ghaedi and his co-workers prepared various mono-, bi-, and tri-metallic nanoparticles (palladium, silver, bismuth−silver, copper−zinc−nickel, and nickel−cobalt−alumina) that were used as an adsorbent for the removal of Congo red.[29]

Synthetic dyes are toxic, nonbiodegradable, and carcinogenic and produce hazardous effects on the environment.[30] The decolorization of triphenylmethane dyes such as crystal violet, methyl violet, malachite green, Coomassie brilliant blue, and gentian violet has acquired increasing attention under various experimental conditions.[5,31,32] Brilliant FCF food dye (blue 1, E133; used as a food colorant) is a synthetic dark blue-colored dye of the triphenylmethane auxochrome category (Scheme 1).

The degradation studies of E133 and Coomassie brilliant blue by AgNPs have been reported under different experimental conditions,[33−35] but the kinetics of decolorization and mineralization of E133 with AgNPs under the UV/$K_2S_2O_8$ system have been neglected. The main aim of this work purpose was to investigate the factors that influenced the photocatalytic and oxidative decolorization of E133 by $K_2S_2O_8$ and $NaBH_4$ with AgNPs as an activator and/or catalyst. The factor studies are the oxidant doses, initial E133 concentration, and effect of AgNPs concentration, pH, and temperature. We investigated the E133 decolorization followed by mineralization under the UV/$K_2S_2O_8$ system. The kinetics of decolorization and mineralization were discussed and then a mechanism for the degradation was proposed for the first time.

https://doi.org/10.1021/acsomega.1c04501
ACS Omega 2021, 6, 27510−27526

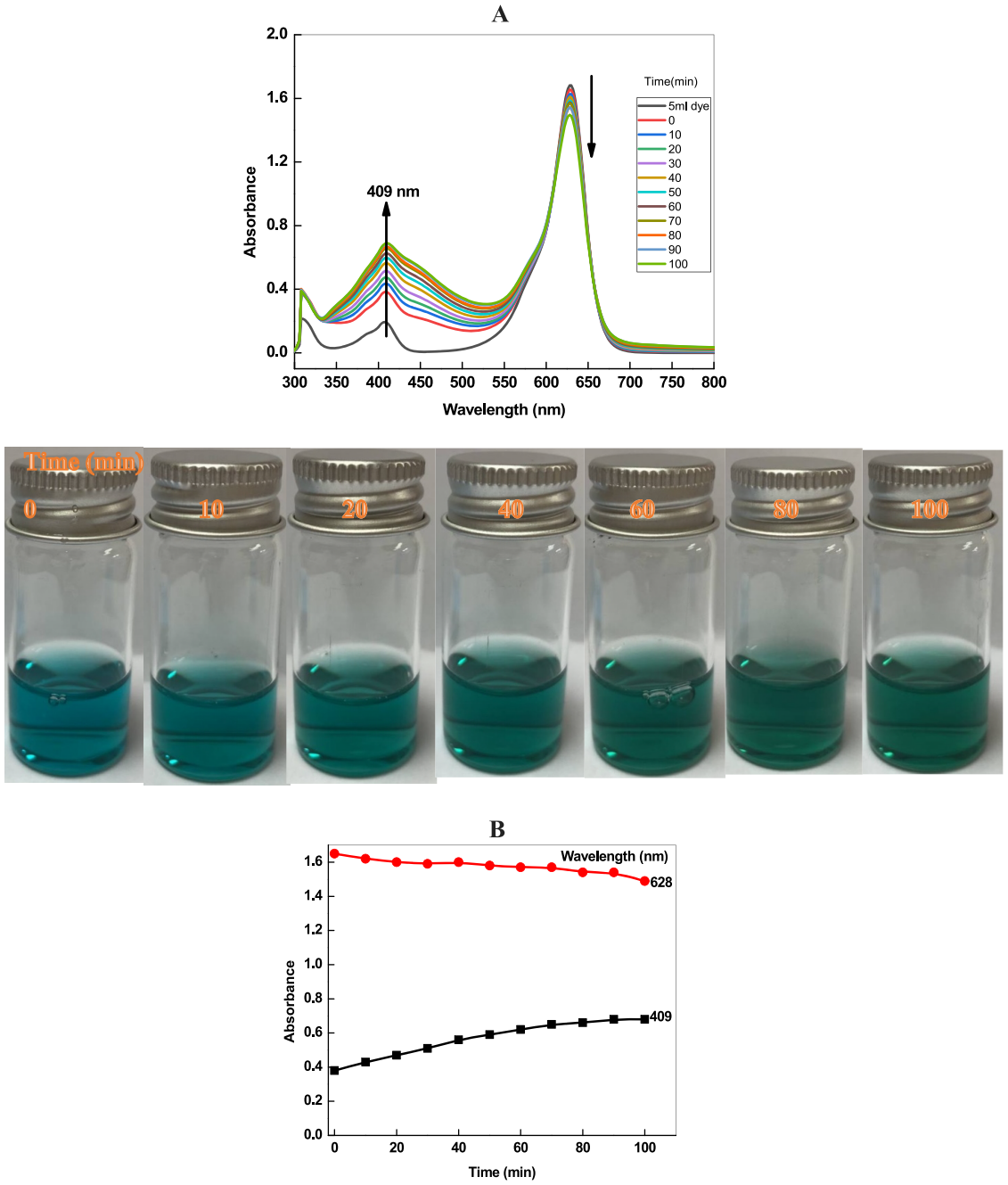

Figure 2. UV−visible spectra and optical images (A) and reaction−time profile (B) of decolorization of E133 by AgNPs without $K_2S_2O_8$ under UV irradiation as a function of time at 30 °C. Reaction conditions: [AgNPs] = 0.01 g/L, [dye] = 3.9×10^{-5} mol/L, and [$K_2S_2O_8$] = 0.0 mol/L.

RESULTS AND DISCUSSION

Preliminary Studies. In the first set of experiments, the UV−visible spectra of E133 were recorded for different dye concentrations. These results are given in Figure 1A, which shows that the E133 exhibits three absorption peaks at 309, 405, and 628 nm in an aqueous solution. The absorbance of the 628 nm peak was immense compared to those of others. At a higher E133 concentration ($\geq 4.68 \times 10^{-5}$ mol/L), the shape of the 628 nm peak has been changed entirely, which might be due to the self-aggregation of dye molecules.[36−38] A Beer−Lambert plot was drawn between the absorbance and concentrations of E133 to determine the molar extinction coefficient (ε). Interestingly, the absorbance−concentration plot deviated from the linearity at higher E133 concentrations (Figure 1B). Therefore, the value of ε was calculated from the linear part of the plot and found to be 4.8×10^4 L/mol/cm at 30 °C. The relation between the absorbance A_{628} and the concentration of commercial E133 is $A_{628} = 4.8 \times 10^4 \times$ [E133] (mol/L), with $R^2 = 0.997$. For the decolorization experiments, the lower E133 concentration ($\leq 3.9 \times 10^{-5}$ mol/L) was used in the entire study. The AgNPs were prepared by using hydrazine and CTAB as a reducing and stabilizing agent at 30 °C. In a typical experiment, the aqueous solution of $AgNO_3$ (1.25 mM) was added into a reaction vessel containing hydrazine (5.0 mM) and CTAB (0.8 mM) and stirred with a magnetic stirrer. The UV−visible spectra of resulting orange-colored silver sols were recorded at different time intervals. The resulting AgNPs exhibited a sharp absorption peak at 440

https://doi.org/10.1021/acsomega.1c04501
ACS Omega 2021, 6, 27510−27526

Scheme 2. Adsorption of E133 on the Surface of AgNPs

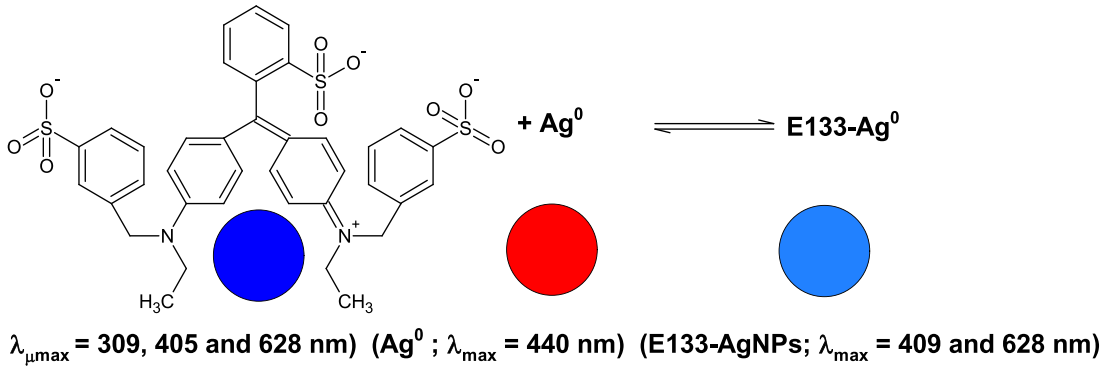

nm, indicating the reduction of Ag^+ ions into metallic Ag^0, and the sols were stable for ca. 1 month (Figure 1C).[39] No precipitates and any type of turbidity appeared. To determine the effect of sodium thiosulfate on the stability of AgNPs, the UV−visible spectra of AgNPs were recorded for different $Na_2S_2O_3$ concentrations. The absorbance and surface plasmon resonance (SPR) peak position of AgNPs remained unchanged at 440 nm even for ca. 24 h in the presence of $Na_2S_2O_3$ (from 0.50×10^{-6} to 2.5×10^{-6} mol/L). The AgNPs were also stable for ca. 1 week with $NaBH_4$ (20×10^{-5} mol/L).[40] Figure 1D shows a transmission electron microscopy (TEM) image of the AgNPs, which are spherical and polydispersed and have a diameter ranging from 5 to 80 nm. Inspection of the TEM image clearly indicates that the various small NPs are aggregated to each other, and large-size NPs are formed. The solid AgNPs were separated through centrifugation, washed with distilled water, dried at room temperature, stored in an amber glass-colored bottle to protect from light, and used as a catalyst and/or as an activator to the decolorization of E133 under different experimental conditions.

Effect of UV Light on E133 Decolorization. It has been established that the $S_2O_8^{2-}$ anion was activated with heat, UV light, transition metal ions, and metal NPs, producing a $SO_4^{\cdot-}$ radical, which is a stronger oxidant than the $S_2O_8^{2-}$ anion. Therefore, a control experiment was performed in the presence of UV light irradiation without $K_2S_2O_8$. In a typical kinetic run, the 3.9×10^{-5} mol/L concentration of E133 was mixed with AgNPs (0.02 g/L) and irradiated under UV light, and the UV−visible spectra were recorded at different time intervals. Figure 2 shows that only UV light was not sufficient for the decolorization of E133. There was no observable color change with UV irradiation for ca. 100 min of reaction time (Figure 1, optical images). Surprisingly, the absorbance was increased at 409 nm with increasing reaction time (Figure 2, UV−visible spectra), and the intensity at 628 nm was slightly decreased (from 1.65 to 1.49). Under UV light irradiation, there was 9.6% decolorization of E133 at 628 nm with 100 min of reaction time. The increase in absorbance at 409 nm (from 0.38 to 0.68; Figure 2B) can be rationalized due to the adsorption of E133 onto the positive surface of AgNPs (Henglein reported the formation of Ag_4^{2+} as a stable species of AgNPs in an aqueous solution even in the absence of a stabilizing agent[41]) through the negative $-SO_3^-$ of E133 (Scheme 2).

As presented in Figure 1A,C, the spectrum of E133 shows the three absorption peaks at 309, 405, and 628 nm, whereas the AgNPs display an SPR band at 440 nm. Interestingly, a new band at around 409 nm in the absorption of AgNPs in complex with E133 (Figure 2)[38] might be due to the changes in surface plasmonic properties of AgNPs and not from the dye molecule.[42] On the other hand, no decolorization of E133 was observed with increasing $K_2S_2O_8$ concentrations ranging from 0.75×10^{-3} to 5.0×10^{-3} mol/L under a similar E133 concentration, pH (5.5), and temperature (30 °C) in the absence of UV light.

Effect of the UV/$K_2S_2O_8$ System on E133 Degradation. Effect of $K_2S_2O_8$. Figure 3A shows the optical images of a reaction mixture containing AgNPs and E133 as a function of time. We did not observe the appearance of any type of turbidity and/or precipitate for ca. 60 min, which suggests that the E133 was stable with AgNPs at room temperature. E133 was adsorbed on the surface of AgNPs with physical and chemical interactions. To gain insight into the combined effect of $K_2S_2O_8$ and UV light, the UV−visible absorption spectrum changes in the AgNPs-E133 solution were observed, and corresponding spectral and optical images are shown in Figure 3B. Interestingly, the absorption intensity of E133 became weaker along with the reaction time. The blue color of E133 disappeared completely (Figure 3B, optical images), and 90% decolorization was observed in 30 min with the UV/$K_2S_2O_8$ ([$K_2S_2O_8$ = 3.75 mM]) treatment system, which indicates that UV/$K_2S_2O_8$ was superior to UV alone in terms of the dye removal efficiency in the presence of an activator. A careful observation of Figure 3B revealed that, initially, the reaction has a time lag to observe any visible change in the absorbance value, i.e., the induction time. The absorbance of E133 decreases (from 1.67 to 0.03) at 628 nm within 60 min, and the blue color changes to almost colorless. The E133 degradation was calculated and found to be 98%. On the other hand, the absorbance changes from 0.4 to 0.35 with time at 408 nm (Figure 3B, inset), and no sharp SPR band of AgNPs appeared at 440 nm after the complete discoloration of E133 in 60 min. The degradation of E133 and oxidative dissolution of AgNPs occurred simultaneously under UV/$K_2S_2O_8$ treatment due to the activation of persulfate by AgNPs. Kaur et al. also observed the color change of AgNPs and AuNPs after the addition of Fe_2O_3 NPs.[27] These NPs have strong complex-forming efficiency with Fe_2O_3 NPs.

From plots of absorbance at 628 nm, $A_0 - A_t$, and $\ln(A_0/A_t)$ versus time (Figure 4A−C), it may be concluded that the decolorization has an induction period and then the rate increases with time. The extent of induction period depends on the $K_2S_2O_8$ concentrations.[25] The decolorization follows excellent pseudo-first-order kinetics. The effect of reaction time on the decolorization extent was studied as shown in Figure 4B. The decolorization extent was presented by

https://doi.org/10.1021/acsomega.1c04501
ACS Omega 2021, 6, 27510−27526

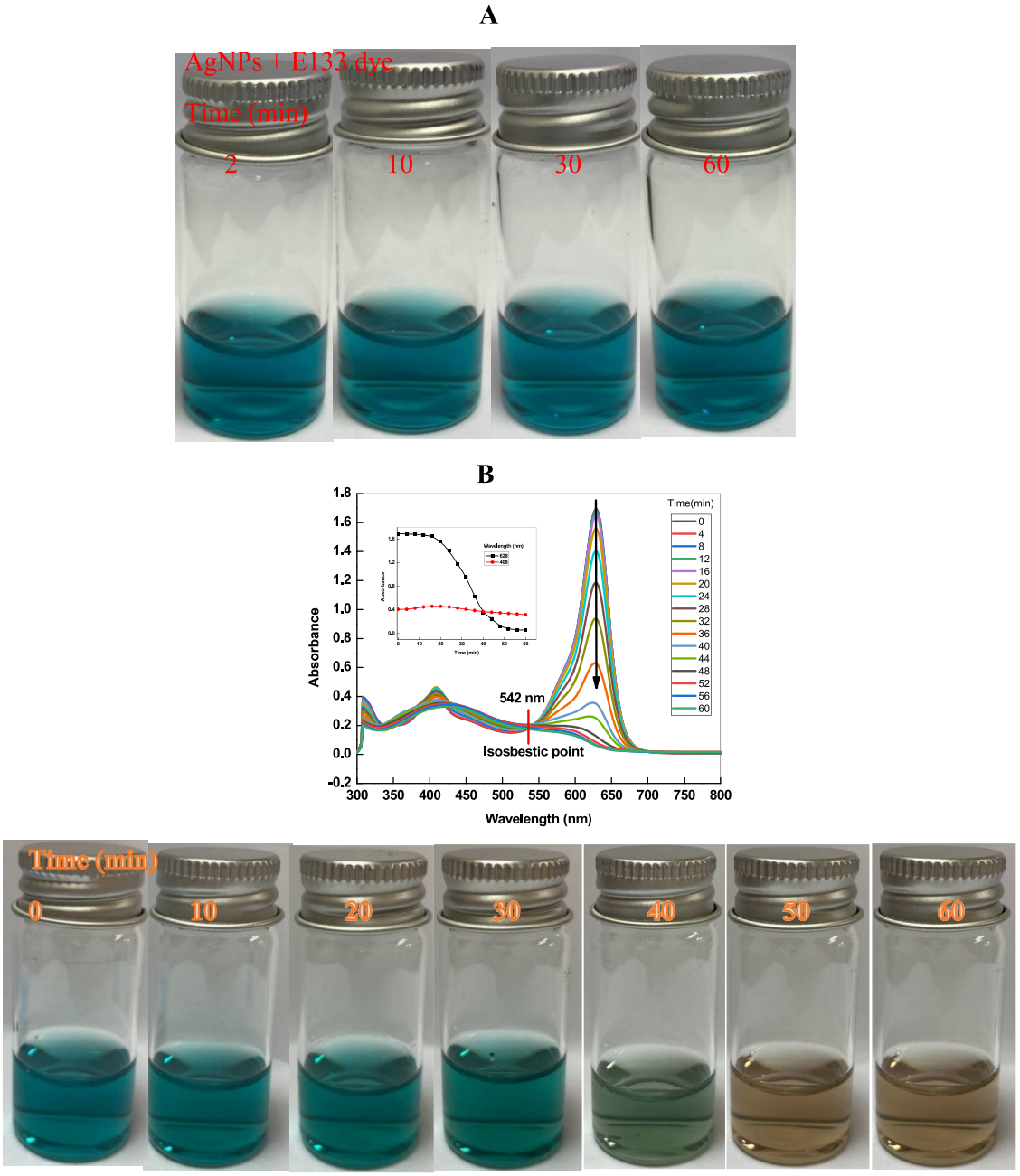

Figure 3. Optical images of AgNPs and E133 (A) and UV−visible spectra and optical images of decolorization of E133 by $K_2S_2O_8$ with AgNPs under UV irradiation as a function of time at 30 °C (B). Inset: Decay of absorbance at 408 and 628 nm with time. Reaction conditions: [AgNPs] = 0.01 g/L, [dye] = 3.9×10^{-5} mol/L, and [$K_2S_2O_8$] = 1.25 mM.

absorbance change ($\Delta A = A_0 - A_t$), where A_0 and A_t are the absorbance of the initial E133 and at reaction time t. It was observed that the ΔA increases rapidly and then approaches an almost constant value after a certain time, which might be due to either complete decolorization of E133 or full consumption of $K_2S_2O_8$. The saturation time was found to be ca. 30 and 60 min for 1.25 and 3.75 mM $K_2S_2O_8$, respectively. The decolorization percentage also depended on the reaction time at different $K_2S_2O_8$ concentrations, i.e., 90% E133 was decolorized within 30 min at 3.75 mM $K_2S_2O_8$ (Figure 4D). Therefore, a $SO_4^{\cdot-}$ radical was generated in the reaction mixture (E133 + $S_2O_8^{2-}$ + Ag^0) by the scission of a peroxide bond by UV light.[19] The resultant $SO_4^{\cdot-}$ undergoes a series of chain reactions, and other oxidants such as $HO^{\cdot}$ and peroxymonosulfate (HSO_4^-) were generated (eqs 1−5).

$$S_2O_8^{2-} + \text{heat/UV} \rightarrow 2SO_4^{\cdot-} \quad (1)$$

$$2SO_4^{\cdot-} \rightarrow 2SO_4^{2-} \quad (2)$$

$$SO_4^{\cdot-} + H_2O \rightarrow SO_4^{2-} + HO^{\cdot} + H^+ \quad (3)$$

$$SO_4^{\cdot-} + HO^{\cdot} \rightarrow HSO_5^- \quad (4)$$

$$SO_4^{\cdot-} + \text{E133} \rightarrow SO_4^{2-} + \text{decolorized E133} \quad (5)$$

$SO_4^{\cdot-}$ (E_0 = 2.6 V) can oxidize E133 via a one-electron transfer step, leading to decolorization of the dyes.[43,44] The

https://doi.org/10.1021/acsomega.1c04501
ACS Omega 2021, 6, 27510−27526

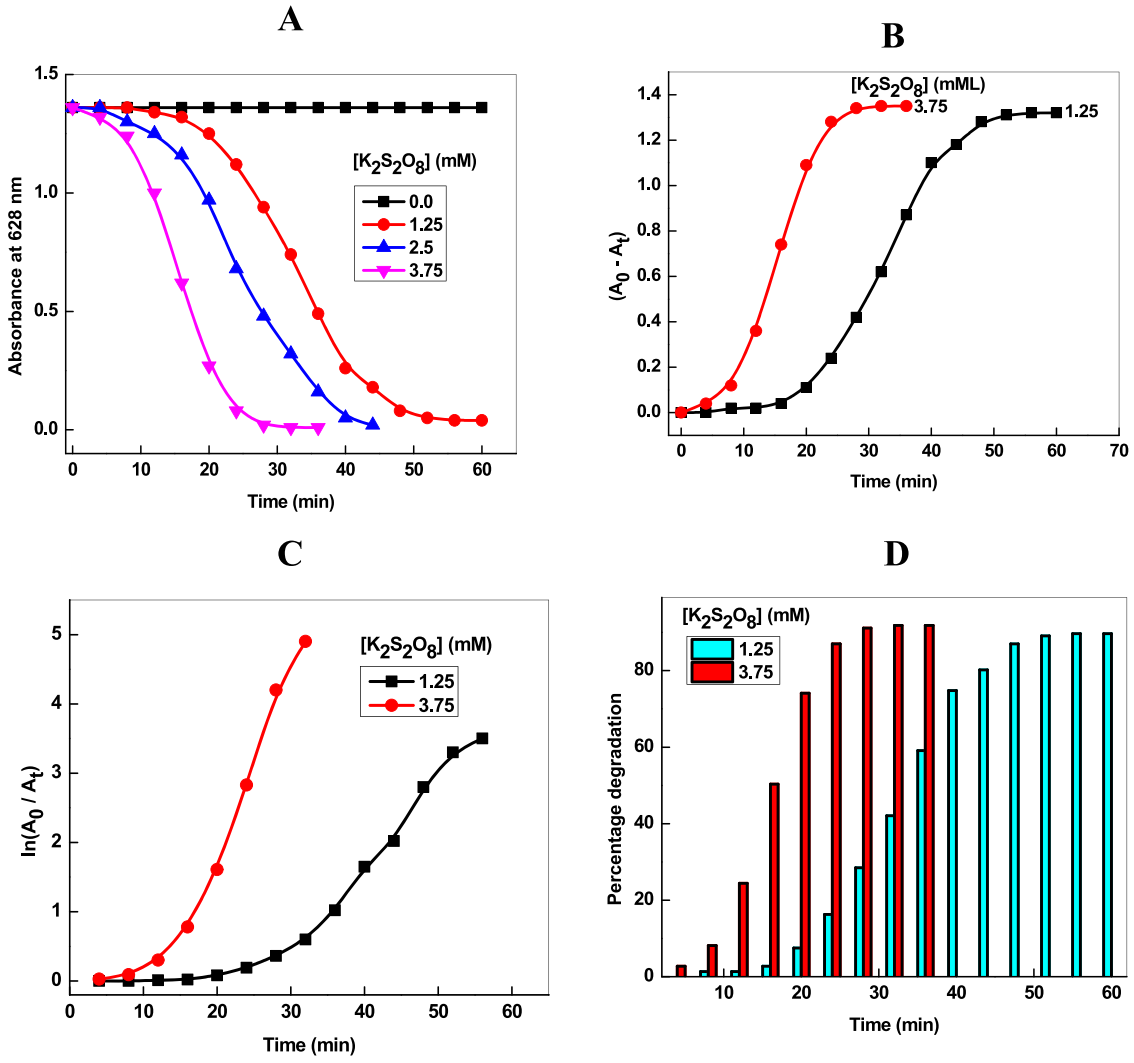

Figure 4. Plots of absorbance decay at 628 nm (A), $A_0 - A_t$ (B), $\ln(A_0/A_t)$ (C), and percentage decolorization versus time to the decolorization of E133 by $K_2S_2O_8$ with AgNPs at 30 °C (D). Reaction conditions: [AgNPs] = 0.01 g/L, [dye] = 3.9 × 10^{-5} mol/L, and [$K_2S_2O_8$] = 1.25 mM.

Table 1. Effects of [E133], pH, [$K_2S_2O_8$], and AgNPs on the Decolorization of E133 with the UV/$K_2S_2O_8$ System at 30 °C

10^5[E133] (mol/L)	[$K_2S_2O_8$] (mM)	[AgNPs] (g/L)	pH	$10^4 k_{obs}$ (s^{-1})
3.1	0.0	0.01	5.5	0.0
3.1	3.75	0.01	5.5	39.7 ± 4.4
3.9	3.75	0.01	5.5	36.1 ± 4.4
4.6	3.75	0.01	5.5	33.6 ± 5.2
5.4	3.75	0.01	5.5	29.8 ± 5.1
3.9	0.75	0.01	5.5	10.5 ± 4.3
3.9	1.25	0.01	5.5	22.9 ± 4.5
3.9	2.5	0.01	5.5	30.2 ± 4.4
3.9	5.0	0.01	5.5	42.1 ± 3.4
3.9	5.0	0.01	5.5	42.1 ± 4.7
3.9	3.75	0.02	5.5	40.2 ± 4.5
3.9	3.75	0.03	5.5	44.6 ± 4.6
3.9	3.75	0.04	5.5	46.5 ± 5.1
3.9	3.75	0.05	5.5	48.2 ± 4.6
3.9	3.75	0.01	3.5	40.2 ± 4.8
3.9	3.75	0.01	8.5	25.2 ± 4.4
3.9	3.75	0.01	10.5	18.5 ± 4.6

values of rate constants were calculated for different $K_2S_2O_8$ concentrations at a fixed E133 concentration, AgNP concentration, pH, and temperature. Table 1 shows that the rate constant of E133 decolorization was increased with $K_2S_2O_8$ from 0.75 to 5.0 mM. However, a further increase in $K_2S_2O_8$ above certain limits decreased the decolorization rate constants. This is mainly because $K_2S_2O_8$ has two different roles during the dye degradation.[45,46] At lower concentrations, the generated $SO_4^{\cdot-}$ will be available to attack on E133 molecules. As a result, the reaction rate increases. On the other hand, $S_2O_8^{2-}$ acts as a $SO_4^{\cdot-}$ radical scavenger instead of a free radical generator at higher concentrations (eqs 6 and 7).

$$S_2O_8^{2-} + SO_4^{\cdot-} \rightarrow SO_4^{2-} + S_2O_8^{\cdot-} \quad (6)$$

$$2SO_4^{\cdot-} \rightarrow S_2O_8^{2-} \quad (7)$$

There is a competition between $S_2O_8^{2-}$ and E133 to react with a $SO_4^{\cdot-}$ free radical in excess of $K_2S_2O_8$. The $S_2O_8^{2-}$ reactivity was higher toward $SO_4^{\cdot-}$, decreasing the free radical concentration in solution, which in turn decreases the rate of decolorization at higher $K_2S_2O_8$ concentrations.[47]

Effect of Dye and pH. The effect of initial E133 concentration on the rate of decolorization efficiency in the

https://doi.org/10.1021/acsomega.1c04501
ACS Omega 2021, 6, 27510−27526

Table 2. Effect of Temperature on the Decolorization of E133 under Various Reaction Conditions

reaction system	temperature (°C)	$10^4 k_{obs}$ (s^{-1})	E_a (kJ/mol)	$\Delta H^{\#}$ (kJ/mol)	$\Delta S^{\#}$ (J/K/mol)
E133/$K_2S_2O_8$	30	no reaction			
	40	no reaction			
	50	2.5 ± 5.0	57.4 ± 4.4	54.8 ± 4.6	−139.1 ± 4.6
	60	4.6 ± 4.0			
	70	9.2 ± 5.0			
E133/AgNPs	30	no reaction			
	40	no reaction			
E133/AgNPs/$K_2S_2O_8$	30	8.7 ± 4.0	30.6 ± 4.7	28.1 ± 4.8	−128.8 ± 4.8
	40	16.2 ± 5.0			
	50	32.4 ± 5.0			
	60	64.4 ± 4.0			

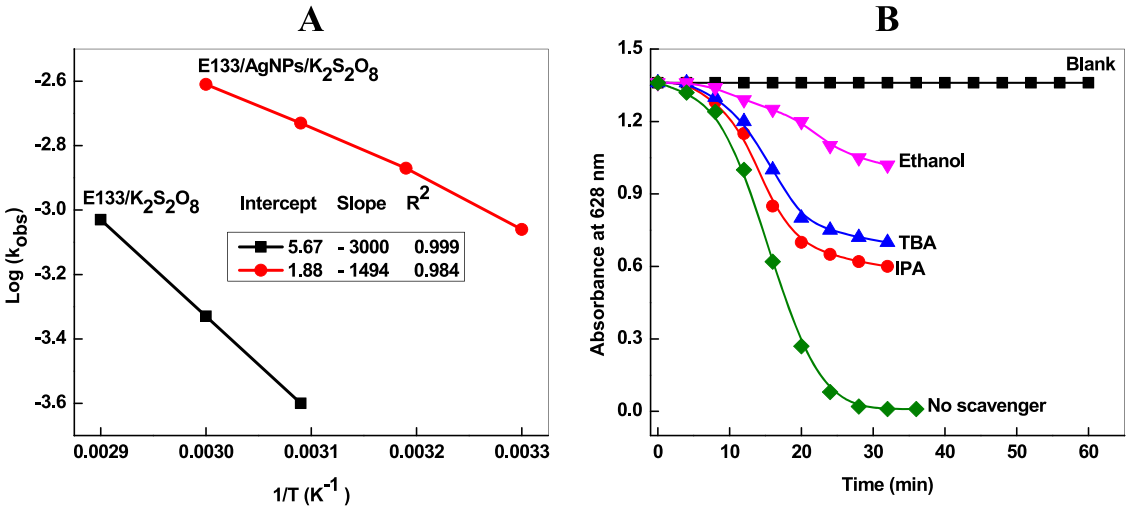

Figure 5. Arrhenius plot (A) and effects of scavenger on the decolorization of E133 by $K_2S_2O_8$ with AgNPs at 30 °C (B). Reaction conditions: [AgNPs] = 0.01 g/L, [dye] = 3.9 × 10^{-5} mol/L, and [$K_2S_2O_8$] = 1.25 mM.

UV/$K_2S_2O_8$ system with AgNPs was monitored in the range of 3.1 × 10^{-5} to 5.4 × 10^{-5} mol/L while maintaining the other parameter constant (Table 1). It can be seen that the rate of decolorization decreases as the initial dye concentration increases at a constant $K_2S_2O_8$ concentration, which might be due to the fact that the high concentration of E133 would consume more $SO_4^{\cdot-}$. On the other hand, the penetration of photons entering into the reaction mixture decreases due to the high concentration of E133. As a result, the solution became more impermeable to the UV radiation due to the inter-filter effect. Finally, the $SO_4^{\cdot-}$ concentration decreases, which in turn decreases the rate of decolorization. The solution pH is an important parameter and has significant impact on the dye degradation. Therefore, the effect of pH (3.5, 5.5, 8.5, and 10.5) was investigated on the decolorization of E133. The results of pH dependency on the rate of decolorization are summarized in Table 1, which shows that the decolorization of E133 decreased with the increase in the pH value from 5.5 to 10.5. It was observed that the E133 was completely removed after 25 min at pH 3.5. The percentage decolorization values of E133 were 90, 93, 55, and 45% at pH 3.5, 5.5, 8.5, and 10.5, respectively. At pH 5.5, the percentage degradation was higher than that at pH 3.5, indicating the scavenging of $SO_4^{\cdot-}$ in acidic media.[48] The generation of $SO_4^{\cdot-}$ was increased in acidic solution (i.e., pH = 3.5) due to acid catalyzation (eqs 12 and 13), which leads to increases in the concentration of $SO_4^{\cdot-}$ in solution, and scavenging of $SO_4^{\cdot-}$ occurs simultaneously via eqs 8 and 9.

$$S_2O_8^{2-} + H^+ \rightarrow HS_2O_8^- \quad (8)$$

$$HS_2O_8^- \rightarrow H^+ + SO_4^{2-} + SO_4^{\cdot-} \quad (9)$$

In alkaline solution (pH ≥ 8.5), $SO_4^{\cdot-}$ was unstable, started to decompose, and transformed rapidly into HO· due to the base activation mechanism of persulfate for the generation of $SO_4^{\cdot-}$ in the aqueous, neutral, and alkaline media (eq 10).[49,50]

$$S_2O_2^{8-} + 2H_2O \rightarrow SO_4^{\cdot-} + 2SO_4^{2-} + O = O^{\cdot-} + 4H^+ \quad (10)$$

$SO_4^{\cdot-}$ reacts with HO^- and immediately generates HO· in basic conditions (eq 11), which has little reduction potential than $SO_4^{\cdot-}$. The reactivity of $HO^{\cdot}$ was lower in solution due to the existence of $SO_4^{2-\cdot}$.[51] As a result, the percentage degradation and decolorization rate of E133 were decreased at pH ≥ 8.5 due to the recombination of both reactive species, $SO_4^{\cdot-}$ and HO· (eqs 11 and 12).

$$HO^- + SO_4^{\cdot-} \rightarrow SO_4^{2-} + HO^{\cdot} \quad (11)$$

$$HO^{\cdot} + SO_4^{\cdot-} \rightarrow HSO_4^- + \frac{1}{2}O_2 \quad (12)$$

https://doi.org/10.1021/acsomega.1c04501
ACS Omega 2021, 6, 27510−27526

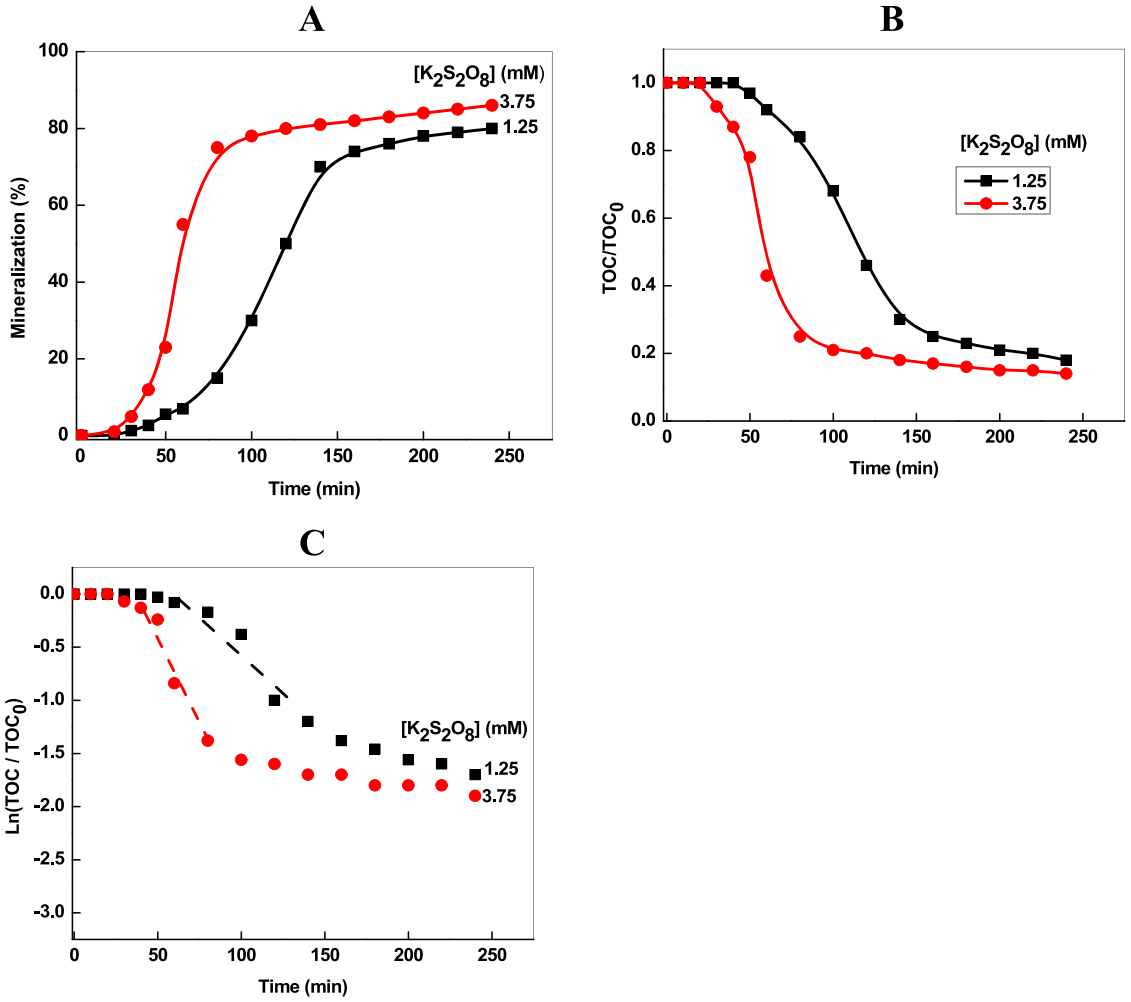

Figure 6. Plot of mineralization % (A), TOC/TOC_0 (B), and $\ln(TOC/TOC_0)$ versus time (C) for the degradation of E133 with AgNPs at 30 °C. Reaction conditions: [AgNPs] = 0.01 g/L and [dye] = 3.9×10^{-5} mol/L.

Table 3. Kinetic Parameters of the Decolorization and Mineralization of E133 under the UV/$K_2S_2O_8$ System

parameter	$[K_2S_2O_8]$ (1.25 mM)	$[K_2S_2O_8]$ (3.75 mM)
k_{obs} (s^{-1})	$22.9 \times 10^{-4} \pm 4.5$	$36.1 \times 10^{-4} \pm 4.4$
R^2	0.994	0.996
k_{TOC}	$1.0 \times 10^{-4} \pm 4.7$	$5.5 \times 10^{-4} \pm 4.9$
R^2	0.930	0.938

Our results are in good agreement with the observations of Hussain et al.,[23] Xu and Li,[44] and Furman et al.[50] regarding the degradation of toxic dyes and water pollutants with persulfate.

Effect of AgNPs and Temperature. Using 3.7 mM $K_2S_2O_8$, different concentrations of AgNPs (0.01 to 0.05 g/L) were used to investigate their effect on E133 decolorization (3.75×10^{-5} mol/L) at pH = 5.5 and 30 °C. It was observed that the AgNPs and/or $K_2S_2O_8$ only do not provide any decolorization effect in the absence of UV light as shown by the control experiment in Figure 4A. The decolorization rate increased with increasing AgNPs (Table 1). The higher concentration of AgNPs provides more sites for $SO_4^{\cdot-}$, thereby increasing the reaction rate. Henglein reported the formation of Ag_4^{2+} of AgNPs in an aqueous solution (eqs 13 and 14).[41]

$$Ag^0 + Ag^+ \rightarrow Ag^0 - Ag^+ \quad (13)$$

$$2Ag^0 - Ag^+ \rightarrow Ag_2^+ - Ag_2^+ \quad (Ag_4^{2+}) \quad (14)$$

When the AgNP concentrations were varied at 0.01, 0.02, 0.03, 0.04, and 0.05 g/L, the decolorization rates were 36.1×10^{-4}, 40.2×10^{-4}, 44.6×10^{-4}, 46.5×10^{-4}, and 48.2×10^{-4} s^{-1}, respectively, which might be due to the higher production of $SO_4^{\cdot-}$. Thus, $S_2O_8^{2-}$ ions were adsorbed on the surface of AgNPs through electrostatic interactions and acted as an activator for the generation of $SO_4^{\cdot-}$ (eqs 15 and 16).[52−54]

$$S_2O_8^{2-} + (Ag_2^+ - Ag_2^+) \rightarrow Ag^{2+} + SO_4^{2-} + SO_4^{\cdot-} + Ag_2^+ + Ag^0 \quad (15)$$

$$S_2O_8^{2-} + (Ag_2^+ - Ag_2^+) \rightarrow [Ag^{II}(SO_4)]^+ + SO_4^{2-} + Ag_2^+ + Ag^0 \quad (16)$$

Generally, heat has been used as another important parameter to the activation of $S_2O_8^{2-}$.[55] Therefore, the effect of temperature (30, 40, 50, 60, and 70 °C) was studied on the decolorization of E133 by keeping other parameters constant. In the absence of AgNPs, the E133 decolorization was not observed at 30 and 40 °C for the $K_2S_2O_8$/E133 system. As the temperature increases from 50 to 70 °C, the rate significantly increases (Table 2) due to the activation of $S_2O_8^{2-}$ by heat. On

https://doi.org/10.1021/acsomega.1c04501
ACS Omega 2021, 6, 27510−27526

Scheme 3. Decolorization and Mineralization of E133 by AgNPs under UV/$K_2S_2O_8$ Treatment

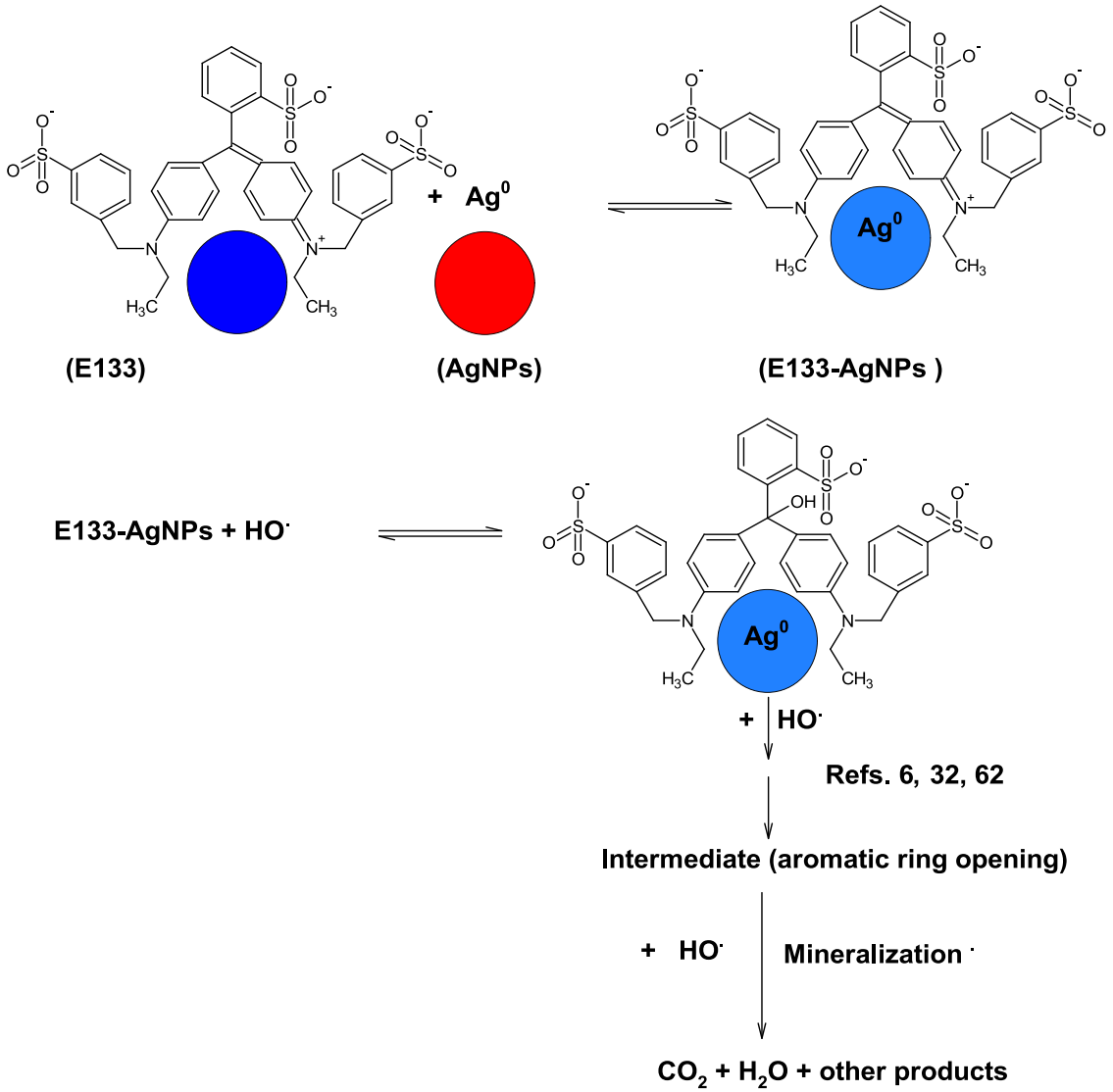

Scheme 4. Dissolution of AgNPs by HO· Generated by $K_2S_2O_8$

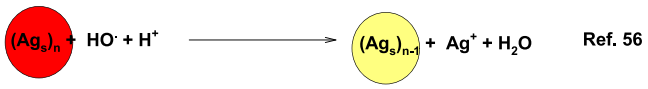

the other hand, the decolorization was observed at 30 °C for the AgNPs/$K_2S_2O_8$ system, indicating the combined effect of heat and AgNPs to the activation of $S_2O_8^{2-}$. The rate constants of E133 decolorization were 12.4×10^{-4}, 24.4×10^{-4}, 40.2×10^{-4}, and 76.0×10^{-4} s^{-1} at 30, 40, 50, and 60 °C, respectively. The E133 removal efficiency by AgNPs/heat-activated $S_2O_8^{2-}$ was higher than that without AgNPs (Table 2). The activation energy (E_a), enthalpy of activation ($\Delta H^{\#}$), and entropy of activation ($\Delta S^{\#}$) for the reaction were calculated by using Arrhenius (eq 17) and Eyring (eq 18) equations.

$$\ln k_{obs} = -\frac{E_a}{R}\cdot\frac{1}{T} + \ln A \quad (17)$$

$$\ln\left(\frac{k_{obs}}{T}\right) = -\frac{\Delta H^{\#}}{R}\cdot\frac{1}{T} + \ln\frac{k_b}{h} + \frac{\Delta S^{\#}}{R} \quad (18)$$

where k_{obs}, A, R, T, and k_b are the rate constant, Arrhenius frequency factor, gas constant, temperature (in Kelvin), and Boltzmann constant, respectively. A good linear relationship was observed between the ln k_{obs} versus $1/T$ (Figure 5A). The E_a values for the reaction were 57.4 and 30.6 kJ/mol, respectively, for heat and AgNPs/heat-activated $S_2O_8^{2-}$. The decrease in the E_a in the presence of AgNPs relative to that in the absence of AgNPs proves their catalytic effect (Table 2).

Effect of Scavengers. To identify the dominating role of radical species ($SO_4^{\cdot-}$ and $HO^{\cdot}$) in the AgNPs/$K_2S_2O_8$ system, ethanol, isopropyl alcohol (IPA), and tertiary butyl alcohol (TBA) were used as quenchers.[56−58] The quenching experiments were carried out with the addition of these quenchers (0.01 mol/L) under the similar conditions as those described previously (Figure 4). The results clearly shows that the E133 decolorization was decreased by the addition of all alcohols (Figure 5B). For example, decolorization was 92% in the absence of any scavenger. However, 54, 47, and 22% decolorization was observed in the presence of IPA, TBA,

https://doi.org/10.1021/acsomega.1c04501
ACS Omega 2021, 6, 27510−27526

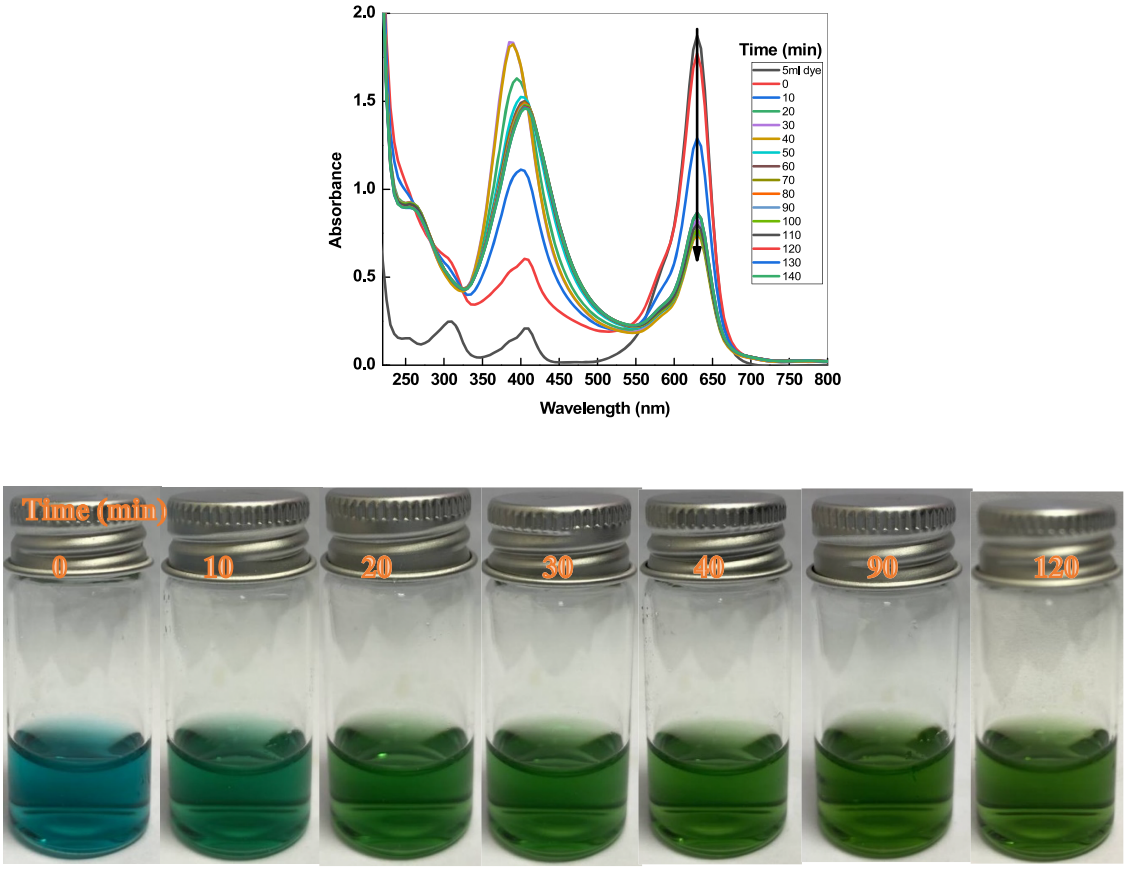

Figure 7. UV−visible spectra and optical images of decolorization of E133 by $NaBH_4$ with AgNPs as a function of time at 30 °C. Reaction conditions: [AgNPs] = 0.01 g/L, [dye] = 3.9 × 10^{-5} mol/L, and [$NaBH_4$] = 1.25 mM.

and ethanol, respectively. The reaction was completely quenched by TBA, which is a more effective quenching agent for $SO_4^{\cdot-}$ (quenching rate = 1.6 × 10^7 to 7.7 × 10^7 mol^{-1} s^{-1}).[57] It reacts much slower with HO· (quenching rate = 1.2 × 10^5 to 2.8 × 10^5 mol^{-1} s^{-1}).[58] These results indicate that the $SO_4^{\cdot-}$ radicals are indeed the primary species generated by the AgNPs/$K_2S_2O_8$ system. However, the role of $HO^{\cdot}$ cannot be ruled out completely because ethanol also quenched the decolorization of E133.[59]

Total Organic Carbon Disappearance. The decolorization and mineralization are the two different paths of the complete dye degradation into CO_2 and water. The various short- and/or long-lived intermediate(s) were formed during the decolorization of dye, which may be more toxic than the original dye. Colonna et al.[60] and Aleboyeh et al.[61] suggested that the final step toward the mineralization of dye starts only when decolorization is nearly complete. The kinetic experiments were also performed to evaluate the removal of the TOC ratio of the reaction mixture at a fixed initial E133 concentration of 3.75 × 10^{-5} mol/L, AgNP concentration of 0.01 g/L, and pH 5.5 at 1.25 and 3.75 mM $K_2S_2O_8$. Figure 6 shows the corresponding change in TOC with time. TOC versus time plots clearly show that after an initial time of constant (induction time), a relatively fast decrease occurs (auto-acceleration). During the first 10, 20, and 40 min, ca. 3 to 12% TOC degradation was observed in solution for both $K_2S_2O_8$ concentrations, indicating that the TOC removal is very slow in the colored solution (Figure 6A). The TOC removal increased with increasing time, and 80% TOC was removed after 100 min reaction time for 3.75 mM $K_2S_2O_8$. Our results are in accordance to the observations of Colonna et al.[60] and Aleboyeh et al.[61] regarding the TOC of dye degradation. The TOC complete removal time depends on the concentration of $K_2S_2O_8$.

Figure 6B shows the TOC ratio (TOC/TOC_0) in E133 solutions as a function of time for two different $K_2S_2O_8$ concentrations. The TOC decay follows the apparent first-order kinetics after the decolorization time (eq 19).

$$-\frac{\mathrm{d}TOC}{\mathrm{d}t} = k_{TOC}\cdot TOC \tag{19}$$

The values of k_{TOC} are calculated from the slope of the final parts of the ln(TOC/TOC_0) versus time and are summarized in Table 3, which indicates that the mineralization reaction rate was very sensitive to the initial concentration of $K_2S_2O_8$. The k_{TOC} rate constants are much lower than those of k_{obs} (rate of decolorization), suggesting that the initial reactive radical attack on the carbon of the E133 molecule leads to the formation of an intermediate (Scheme 3), which maintains the basic aromatic triphenylmethane structure of E133. Further reactions with $SO_4^{\cdot-}$ and/or $HO^{\cdot}$ lead to the cleavage of benzene rings into the smaller organic molecules. The constant level of TOC in Figure 6C after extended irradiation of time suggests that the E133 does not completely mineralize into CO_2 and water under our reaction conditions.

Mechanism of E133 Degradation. Figure 3B shows the decolorization of E133 under treatment with the AgNPs/$K_2S_2O_8$/UV system at 30 °C. The blue color and absorbance intensity of E133 became weaker along with the reaction time, the entirety of the spectra in the UV−visible decreased, and

https://doi.org/10.1021/acsomega.1c04501
ACS Omega 2021, 6, 27510−27526

Scheme 5. Interaction of E133 with AgNPs in the Presence of $NaBH_4$

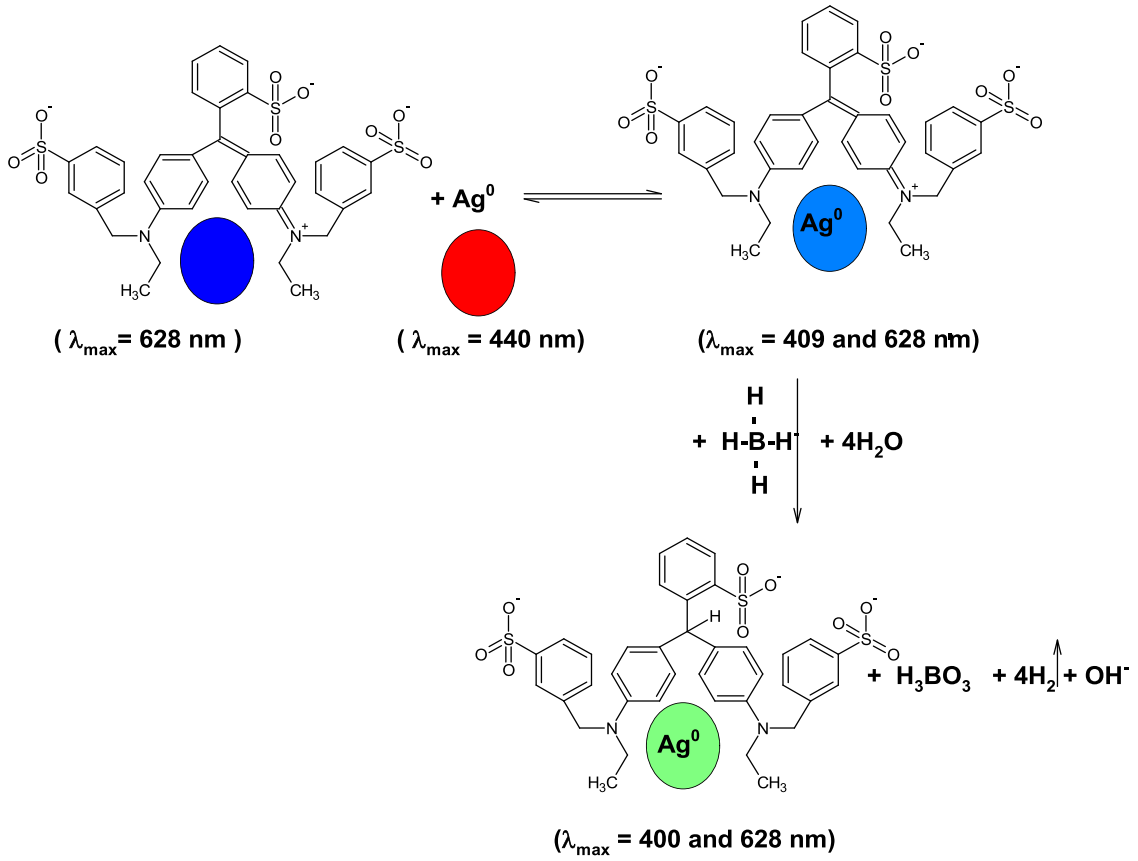

the blue color disappeared completely. The decrease in absorbance in the visible region at 628 nm may be responsible for the oxidative degradation of E133 by the generated reactive oxidants ($SO_4^{\cdot-}$ and $HO^{\cdot}$). Inspection of Figure 3B indicates that the UV−visible spectra became featureless within ca. 60 min. In addition, no new absorption peaks occurred near the original maximum. When we see the UV−visible spectrum, an isosbestic point was observed at 542 nm, which clearly indicates the equilibrium between the parent E133 and its degraded products. Surprisingly, the peak position (wavelength maximum) remains constant at 628 nm during the dye degradation for ca. 44 min and 8 min of the reaction time, respectively, for Figure 3B, and no any shift (red and blue) was observed. On the other hand, the polyaromatic rings were also completely destroyed at the initial stage of the process.

Behnajady et al. observed a blue shift in the degradation of malachite green, which is an N-demethylation process.[31] Rayaroth et al. reported the degradation of Coomassie brilliant blue under sonochemical treatment in the presence of $K_2S_2O_8$.[32] They identified the formation of 13 transformed products as an intermediate during the 10 min of the process and suggested that most of the products were formed mainly due to the attack of HO· via two different mechanisms. Gosetti et al.[62] reported the degradation of E133 by using different $K_2S_2O_8$/dye molar ratios under natural sun light irradiation and suggested the formation of various intermediates under different ratios of dye/persulfate. Li and his co-workers reported the photodegradation of cationic triarylmethane dyes (crystal violet and fuchsin basic) under visible irradiation in TiO_2.[6] They suggested that the dyes were photodegraded via two competitive mechanisms: N-demethylation and the destruction of the conjugated structure. E133 (triphenylmethane dye) is a highly aromatic compound and it has many attacking sites. Therefore, the addition of $HO^{\cdot}$ is more favorable than the N-demethylation process during the initial stages of the degradation.[32] From Figure 3B, we conclude that the AgNP-activated photocatalytic decolorization of E133 by $K_2S_2O_8$ occurs via destruction of the whole conjugated structure of the dye.[6] The disappearance of absorbance peaks at 628 and 409 nm might be due to the simultaneous decolorization of E133 and dissolution of AgNPs under UV/$K_2S_2O_8$ treatment. On the basis of these results and data available in the literature, Schemes 3 and 4 are proposed for the degradation of E133 (decolorization and mineralization) and dissolution of AgNPs, respectively.

Effect of $NaBH_4$. $NaBH_4$ is a strong reducing agent and is used for the oxidative degradation of aromatic nitro compounds,[28] methyl orange, eosin yellow,[63] and bromothymol blue[59] in the presence of AgNPs and Ag@Fe as catalysts. Therefore, to gain insight into the decolorization of E133, a series of kinetic experiments were performed with $NaBH_4$ = 0.75 mM to 5.0 mM at fixed concentrations of E133 (3.75×10^{-5} mol/L) and AgNPs (0.01 g/L) at 30 °C. The representative results are summarized in Figure 7 as the UV−visible spectra of dye discoloration and their optical images. The UV−visible spectrum of E133 shows three absorption peaks at 309, 405, and 628 nm in an aqueous solution (Figure 7, black line). The peak position and intensity remain the same after the addition of $NaBH_4$ for a couple of days. No decolorization of dye was observed with $NaBH_4$. Surprisingly, the dye absorbance decreased very fast after the addition of AgNPs, and the blue color of the reaction mixture

https://doi.org/10.1021/acsomega.1c04501
ACS Omega 2021, 6, 27510−27526

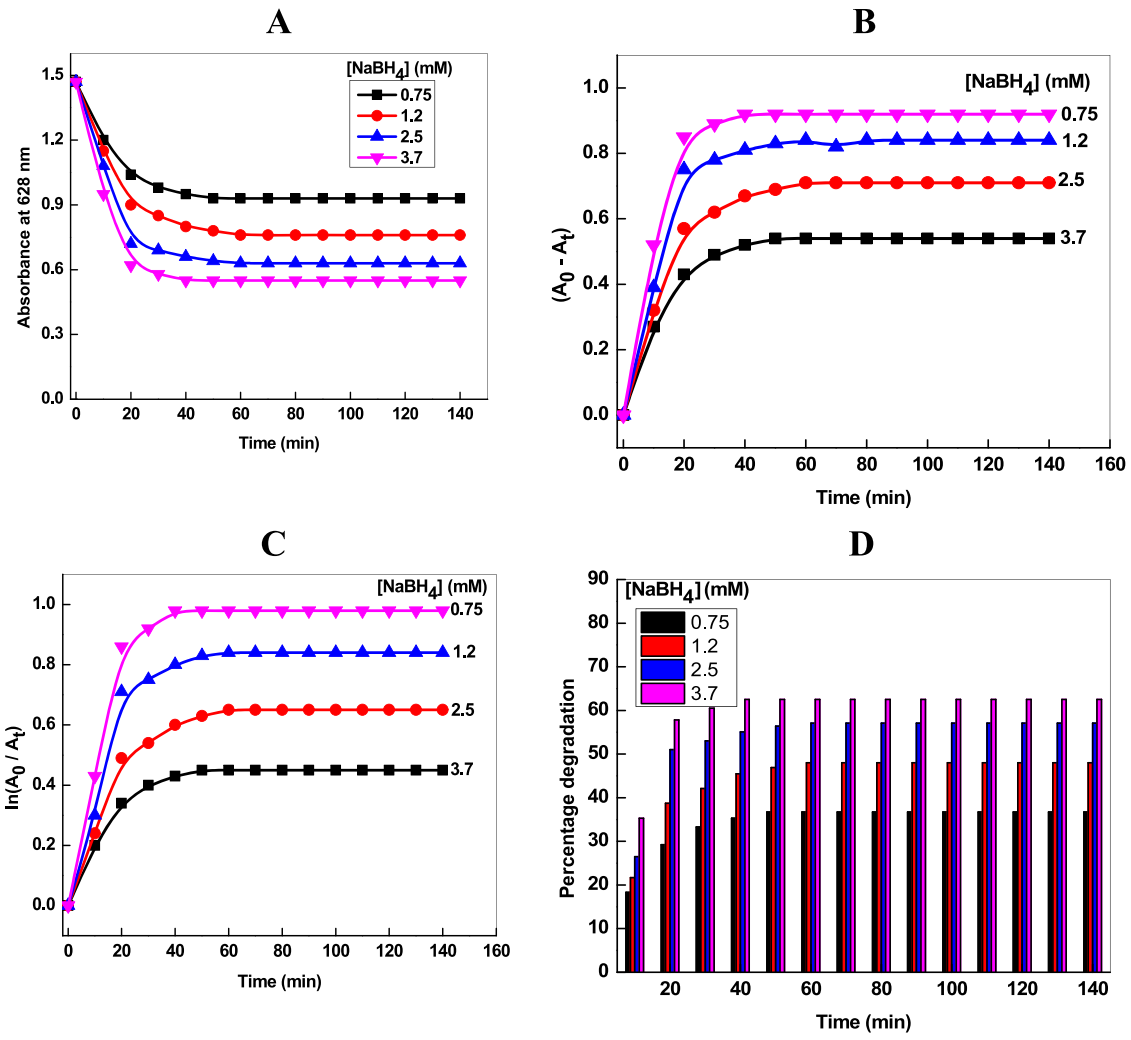

Figure 8. Plots of absorbance decay at 628 nm (A), $A_0 - A_t$ (B), $\ln(A_0/A_t)$ (C), and percentage decolorization versus time to the decolorization of E133 by $NaBH_4$ with AgNPs at 30 °C (D). Reaction conditions: [AgNPs] = 0.01 g/L, [dye] = 3.9×10^{-5} mol/L, and [$NaBH_4$] = 1.25 mM.

became green (Figure 7, optical images). On the other hand, the appearance of a SPR peak at ca. 440 nm due to AgNPs was not noticed. The SPR band position is highly sensitive to the adsorption nucleophile onto the particle surface. AgNPs and E133 formed a complex, and the resulting complex showed two major absorption peaks at 409 and 628 nm. The SPR peak of AgNPs at 440 nm remains masked under the E133 peak. Addition of AgNPs to the reaction solution containing E133 and $NaBH_4$ caused the fading of the blue color of E133. Figure 7 shows that the absorbance at 628 nm decreases, and the blue solution of E133 turns blue-green. The whole UV−visible spectrum changes entirely with increasing time. The successive decrease in the peak height at 628 nm is accompanied by an increase in absorbance at 400 nm with no isosbestic point, indicating the degradation of E133 in the presence of AgNPs. We did not observe the appearance of any new peaks in the UV−visible spectra or an isosbestic point, which ruled out the partial degradation of E133 (N-demethylation and deamination). On the basis of these observations, Scheme 5 is proposed for the interaction of E133 with AgNPs in the presence of $NaBH_4$.

In Scheme 5, BH_4^- and E133 were adsorbed onto the AgNPs. The hydrogen was transferred from BH_4^- to E133 via the surface of AgNPs due to the electron relay effect.[25]

Figure 8 shows the effect of [$NaBH_4$] on the decolorization of E133 in the presence of AgNPs. The decay of absorbance was increased with increasing concentration of $NaBH_4$, and the reaction followed a pseudo-first-order kinetics. The decay was fast initially, and no decolorization was observed after ca. 30 min of the reaction time (Figure 8A). The ΔA ($A_0 - A_t$) versus time plots indicate that 30 min is an optimum time for the decolorization of dye (Figure 8B). The 60% decolorization occurred with 3.75 mM $NaBH_4$ (Figure 8D). For a given $NaBH_4$ concentration, the absorption peak at 404 nm was sensitive for the reaction time, and the absorbance increased initially, then decreased when the time is beyond 30 min, and became constant for ca. 140 min (Figure 9A). The peak was also blue-shifted (from 409 to 394 nm) and red-shifted (from 394 to 404 nm) during the course of the reaction (Figure 9B), which can be explained due to the strong AgNP surface interactions with the nucleophile.[60] The reappearance of the SPR peak at ca. 404 nm with reaction time indicates the catalytic role of AgNPs in the decolorization of E133 by $NaBH_4$. Actually, $NaBH_4$ serves two main purposes, *viz*, fast reduction of E133 and slow dissolution of AgNPs simultaneously.[25,40] The rate of decolorization was increased with $NaBH_4$ (Figure 9C), and the double log−log plot k_{obs} and [$NaBH_4$ or $K_2S_2O_8$] were linear with slope = 0.64 and 0.79,

https://doi.org/10.1021/acsomega.1c04501
ACS Omega 2021, 6, 27510−27526

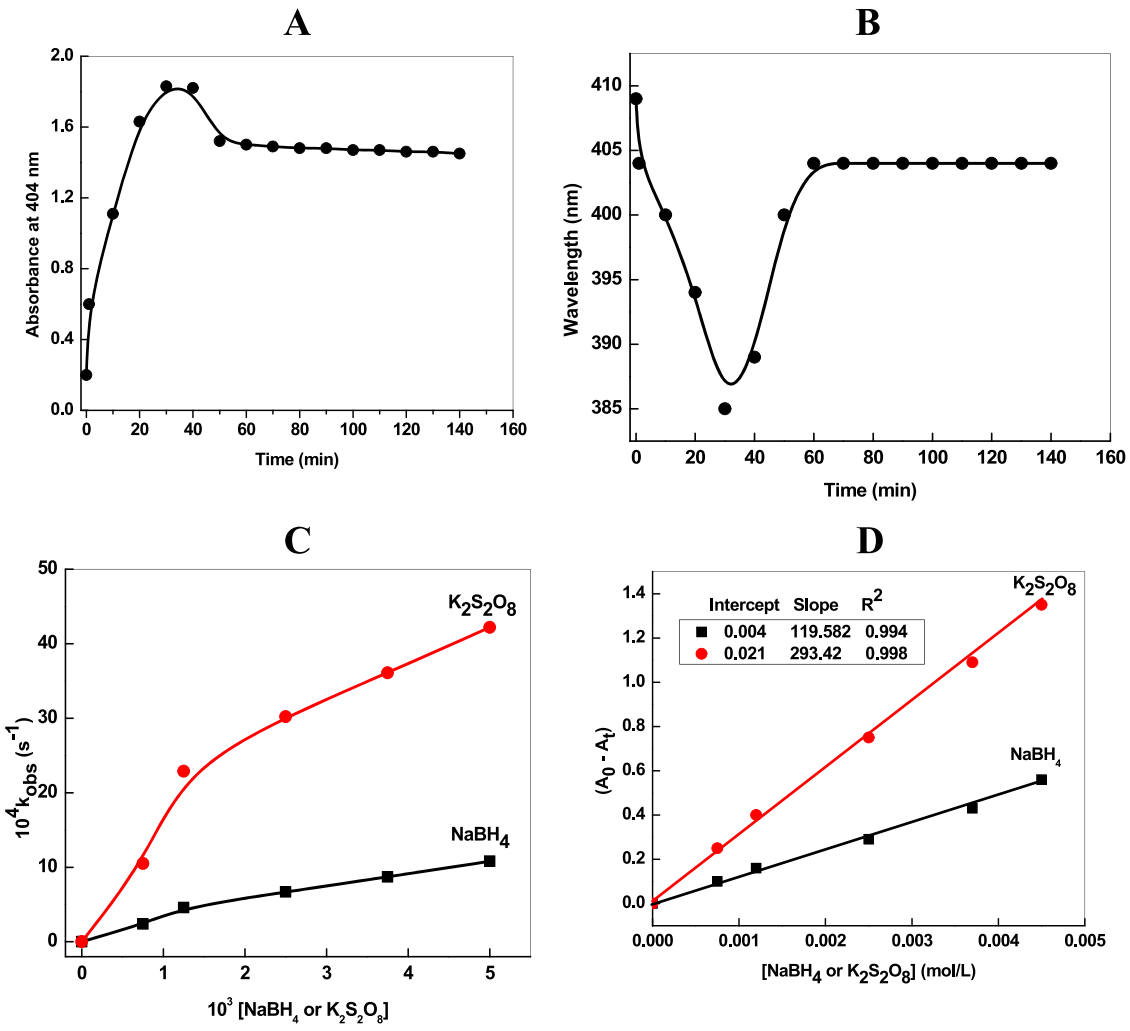

Figure 9. Plot of absorbance decay at 404 nm versus time (A), change in wavelength with time (B), rate constants versus [$K_2S_2O_8$ or $NaBH_4$] (C), and $A_0 - A_t$ versus [$K_2S_2O_8$ or $NaBH_4$] (D) for the decolorization of E133 with AgNPs at 30 °C. Reaction conditions: [AgNPs] = 0.01 g/L, [dye] = 3.9 × 10^{-5} mol/L, and [$NaBH_4$] = 1.25 mM.

indicating the fractional-order first-order kinetics with $NaBH_4$ and $K_2S_2O_8$, respectively.

To compare the reactivity of the $K_2S_2O_8$/AgNPs system, the degradation % and rate constants of different dyes with H_2O_2 and other metal NPs are summarized in Table 4. It is well known that the experimental conditions such as the type of irradiation and metal NPs have significant impact on the degradation of dyes.[64−67] $K_2S_2O_8$/AgNPs is found to be more active to the E133 degradation compared to others. AgNPs activate the peroxide bond of $S_2O_8^{2-}$ and generate the oxygen reactive species ($SO_4^{\cdot-}$ and $HO^{\cdot}$), which might be responsible for the degradation of toxic wastewater pollutants.

Detection Limit of $K_2S_2O_8$ and $NaBH_4$. To determine the detection limit for $K_2S_2O_8$ and $NaBH_4$, the calibration curves were constructed by using the optimize reaction conditions for E133 at 30 °C. A good linear correlation was obtained between ΔA ($A_0 - A_t$) and concentrations of both $K_2S_2O_8$ and $NaBH_4$ (Figure 9D). The following relation was used for the evaluation of the detection limit (DL) (eq 20).

$$\text{detection limit} = \frac{3\sigma}{s} \tag{20}$$

where σ and s are the standard deviation of the blank sample and the slope. These values were calculated from the slopes of Figure 9D and found to be 293.42 and 119.58 for $NaBH_4$ and $K_2S_2O_8$, respectively, and DL values were calculated as 2.42 × 10^{-5} and 1.65 × 10^{-5} mol/L with linear correlation coefficients (R^2) = 0.994 and 0.998, respectively.

CONCLUDING REMARKS

Persulfate can readily degrade and decolorize E133 food colorant dye, adding AgNPs as an activator under thermal and UV irradiation in an aqueous solution. The E133 was completely degraded in the AgNPs/persulfate system within 30 min at a temperature of 30 °C under UV light. The results showed that high AgNP dosages, low pH values (nearly 4 to 5), and low E133 concentrations were more favorable for complete decolorization and mineralization of dye. The decolorization excellently followed the Arrhenius equation with activation energies of ca. 57.4 and 30.6 kJ/mol for E133/AgNPs and E133/AgNPs/$K_2S_2O_8$, respectively, with UV light. Radical scavengers, IPA, TBA, and ethanol demonstrated the responsibility of $SO_4^{\cdot-}$ and $HO^{\cdot}$ radicals in the decolorization of E133. The decolorization of the E133 is of pseudo-first order with respect to the dye concentration. The k_{TOC} reaction rate is much slower than k_{obs}. AgNPs/sodium borohydride is an effective system for the decolorization of E133. The

https://doi.org/10.1021/acsomega.1c04501
ACS Omega 2021, 6, 27510−27526

Table 4. Discoloration Efficiency of E133 under Various Reductants

dye	reaction conditions	degradation	k_{obs} (min^{-1})	ref
Coomassie brilliant blue	ultrasonic degradation; pH = 5.7	90%	0.133	32
Coomassie brilliant blue	ultrasonic degradation; H_2O_2	97%	0.195	32
brilliant blue FCF	$NaBH_4$; AgNPs	97%	0.186	33
Coomassie brilliant blue	$NaBH_4$; AgNPs	92%		34
brilliant blue FCF	$K_2S_2O_8$; zero-valent iron	98.8%		64
brilliant blue FCF	photocatalytic degradation; tungsten-doped TiO_2	93%	0.075	65
Coomassie brilliant blue	UV radiation; H_2O_2	22%	0.041	66
brilliant blue	ultraviolet light-emitting diodes; H_2O_2	100%		67
brilliant blue FCF	UV/$K_2S_2O_8$/AgNPs	98%	0.253	present work
brilliant blue FCF	$NaBH_4$/AgNPs	60%	0.052	present work

decolorization was fast and incomplete with AgNPs/$NaBH_4$. The AgNPs activated the persulfate and BH_4^- ions toward the degradation of dye. The detection limits, 1.65×10^{-5} $K_2S_2O_8$ and 2.4×10^{-5} $NaBH_4$, were determined by using a spectrophotometric method based on the decolorization of E133 food colorant. In the presence of UV/$K_2S_2O_8$, the added AgNPs were fully decomposed along with the decolorization and mineralization of E133, leaving no environmental risk.

EXPERIMENTAL SECTION

Chemicals. Brilliant blue ($C_{37}H_{34}N_2Na_2O_9S_3$; color index = 42,090, 99%) was purchased from Sigma-Aldrich and used as received. $K_2S_2O_8$ (potassium persulfate, 99%), $NaBH_4$ (99%), silver nitrate ($AgNO_3$, ≥99%), cetyltrimethylammonium bromide ($C_{19}H_{42}BrN$, 99%), sodium hydroxide (NaOH, ≥98%), and hydrochloric acid (HCl, 37%) were of analytical grade. Standard HCl (0.1 mol/L) and NaOH (0.1 mol/L) were used for pH adjustment, and all experiments were conducted at 30 °C, unless specified elsewhere, by using double-distilled water as a solvent. The diluted solutions of E133 (ranging from 0.78×10^{-5} mol/L to 7.8110^{-5} mol/L) were prepared from an initial concentration (0.01 mol/L), and a calibration plot was constructed for E133 absorbance at 628 nm and concentrations of E133 to calculate the molar extinction coefficient as well as to verify if the commercial dye obeys Beer–Lambert law.

Preparation and Characterization of AgNPs. The chemical reduction method was used for the preparation of AgNPs with slight modification.[26,68] In the first set of experiments, $AgNO_3$ solution (1.25 mM) was added into a reaction vessel containing cetyltrimethylammonium bromide (0.8 mM) and equilibrated at 30 °C for 20 min. The freshly prepared hydrazine solution (5.0 mM) was added dropwise into the reaction vessel (total volume, 50 mL). The colorless reaction mixture became dark yellow to orange (λ_{max} = 440 nm), indicating the reduction of Ag^+ ions into the metallic Ag^0. The resulting color was stable for ca. 1 month and any type of turbidity and precipitate appeared. In the second set of experiments, hydrazine (1.0 mM), Ag^+ (1.0 mM), and CTAB (0.8 mM) were used for the preparation of AgNPs. The resulting silver sols were analyzed with a Varian Carry 50-UV visible spectrophotometer. The absorbance of silver sols was recorded in the wavelength spectra ranging from 300 to 600 nm. The morphology (size, shape, and size distribution) of the AgNPs was determined using a transmission electron microscope (JEM-1400) equipped with an energy-dispersed X-ray detector, operating at a beam energy of 100 keV. For measurements, samples were prepared by adding droplets of resulting silver sols on the copper–carbon-coated grids (300 meshes) and allowing them to dry at room temperature in a dry box. An X-ray diffractometer (Rigaku, Japan) was used to determine the crystalline nature of the AgNPs. The stability and zeta potential of AgNPs were determined by using the Smoluchowski equation.

Apparatus and Measurements. Stock solutions of $AgNO_3$ (0.01 mol/L), E133 (0.01 mol/L), $NaBH_4$ (0.01 mol/L), and $K_2S_2O_8$ (0.01 mol/L) were prepared in double-distilled water prior to each batch experiment. All of the reactions were carried out in a cylindrical Pyrex reaction vessel (250 mL capacity) with a total reaction volume of 50 mL. For the $K_2S_2O_8$/AgNPs system, the reaction mixture was prepared by mixing a required amount of dye and water on a rotatory shaker at 110 rpm and heated in a water bath for 20 min at 30 °C to attain equilibrium. The decolorization reaction was initiated by mixing a required volume of $K_2S_2O_8$ solution to the mixture solution, which was per-equilibrated at the same temperature followed by the addition of the requited amount of AgNPs. The degradation batch experiments were performed under a UV–visible lamp (12 W, G8 T5 Philips). Solution samples were taken from the reaction vessel at definite time intervals and filtered through a 0.45 μm pore size filter membrane (VWR, USA). Sodium thiosulfate solution was added into the filtrate immediately to quench the oxidation reaction, and the remaining E133 dye was determined by measuring the absorbance at 628 nm (wavelength maximum of dye) on a Varian Carry 50-UV visible spectrophotometer. On the basis of observed results, a linear correlation was established between the $K_2S_2O_8$ concentration and the extent of E133 dye. The same experiments were performed with the required concentration of the $NaBH_4$/AgNPs system to determine the detection limit of $NaBH_4$. For all measurements, duplicate reactions were performed simultaneously. The total organic carbon (TOC) of E133 solution by the catalytic oxidation was determined with a Shimadzu TOC 5000 apparatus.

To determine the order with respect to the $K_2S_2O_8$ concentration, a kinetic study was performed under large excess of different concentrations of $K_2S_2O_8$ (0.75, 1.2, 2.5, 3.7, and 5.0×10^{-3} mol/L) with a fixed concentration of E133 (3.9×10^{-5} mol/L), pH (5.5), and temperature (30 °C). The effect of AgNP dosages on the dye decolorization was studied at 0.01, 0.02, 0.03, 0.04, and 0.05 g/L AgNPs with a fixed concentration of E133, pH, and temperature. To determine the role of temperature on E133 decolorization, the effect of temperature was studied at 30, 40, and 50 °C at other fixed parameters. The effect of E133 concentration (ranging from 3.1×10^{-5} to 5.4×10^{-5} mol/L) was also studied to determine the order with respect to the dye concentration. The pseudo-first-order rate constants were calculated by using the pseudo-first-order rate law (eq 21).

https://doi.org/10.1021/acsomega.1c04501
ACS Omega 2021, 6, 27510−27526

$$k_{obs} = \frac{1}{t}\ln\left[\frac{(A_\alpha - A_0)}{(A_\alpha - A_t)}\right] \quad (21)$$

The rate law for the decolorization reaction is:

$$\text{rate} = k_{obs}[K_2S_2O_8]^n[E133]^m = k_{app}[E133]^m \text{ with } k_{app} = k_{obs}[K_2S_2O_8]^n \quad (22)$$

where k_{obs} is the rate constant determined experimentally. The n and m, respectively, are the order of the reaction with respect to E133 and $K_2S_2O_8$ (or $NaBH_4$). The absorbance is directly proportional to the concentration of dye used in the entire studies. Therefore, k_{obs} will be equivalent to the decolorization rate constant k_{app},[69] according to the Langmuir−Hinshelwood pseudo-first-order kinetic rate law. The percentages of E133 decolorization and mineralization (degradation of an organic compound to its mineral components, i.e., CO_2, H_2O, and other products) were calculated with the following relations (eqs 23 and 24).

$$\text{decolorization (\%)} = \left(1 - \frac{[E133]}{[E133]_0}\right) \times 100 \quad (23)$$

$$\text{mineralization (\%)} = \left(1 - \frac{[TOC]}{[TOC]_0}\right) \times 100 \quad (24)$$

AUTHOR INFORMATION

Corresponding Author

Zoya Zaheer − *Department of Chemistry, Faculty of Science, King Abdulaziz University, Jeddah 21589, Saudi Arabia;* orcid.org/0000-0002-9809-6893; Email: zoya.zaheer@gmail.com, zzkhan@kau.edu.sa

Authors

Abeer Saad Al-Shehri − *Department of Chemistry, Faculty of Science, King Abdulaziz University, Jeddah 21589, Saudi Arabia*

Amell Musaid Alsudairi − *Department of Chemistry, Faculty of Science, King Abdulaziz University, Jeddah 21589, Saudi Arabia*

Samia A. Kosa − *Department of Chemistry, Faculty of Science, King Abdulaziz University, Jeddah 21589, Saudi Arabia*

Complete contact information is available at: https://pubs.acs.org/10.1021/acsomega.1c04501

Author Contributions

Z.Z. designed the experiments and wrote the manuscript. A.S.A.-S. recorded the optical images. S.A.K. and A.M.A. provided the research facilities. Finally, all authors revised and approved the manuscript.

Notes

The authors declare no competing financial interest.

ACKNOWLEDGMENTS

This research work was funded by Institutional Fund Projects under grant number IFPHI-064-247-2020. The authors therefore gratefully acknowledge technical and financial support from the Ministry of Education and King Abdulaziz University, DSR, Jeddah, Saudi Arabia.

REFERENCES

(1) Duxbury, D. F. The photochemistry and photophysics of triphenylmethane dyes in solid and liquid media. *Chem. Rev.* **1993**, *93*, 381−433.

(2) An, S. Y.; Min, S. K.; Cha, I. H.; Choi, Y. L.; Cho, Y. S.; Kim, C. H.; Lee, Y. C. Decolorization of triphenylmethane and azo dyes by Citrobacter sp. *Biotechnol. Lett.* **2002**, *24*, 1037−1040.

(3) García-Río, L.; Leis, J. R.; Mejuto, J. C.; Navarro-Vázquez, A.; Pérez-Juste, J.; Rodriguez-Dafonte, P. Basic hydrolysis of crystal violet in β-cyclodextrin/surfactant mixed systems. *Langmuir* **2004**, *20*, 606−613.

(4) Zollinger, H. *Color Chemistry: Syntheses, Properties, and Applications of Organic Dyes and Pigments*, 2nd rev. ed. John Wiley & Sons, New York, (1991).

(5) Saquib, M.; Muneer, M. TiO_2-mediated photocatalytic degradation of a triphenylmethane dye (gentian violet), in aqueous suspensions. *Dyes Pigm.* **2003**, *56*, 37−49.

(6) Li, X.; Liu, G.; Zhao, J. Two competitive primary processes in the photodegradation of cationic triarylmethane dyes under visible irradiation in TiO_2 dispersions. *New J. Chem.* **1999**, *23*, 1193−1196.

(7) Flury, M.; Flühler, H. Brilliant Blue FCF as a dye tracer for solute transport studies-A toxicological overview. *J. Environ. Qual.* **1994**, *23*, 1108−1112.

(8) Chau, H. W.; Goh, Y. K.; Si, B. C.; Vujanovic, V. An innovative brilliant blue FCF method for fluorescent staining of fungi and bacteria. *Biotech. Histochem.* **2011**, *86*, 280−287.

(9) Staiger, F. A.; Peterson, J. P.; Campbell, D. J. Variations on the "Blue-Bottle" demonstration using food items that contain FD&C Blue #1. *J. Chem. Educ.* **2015**, *92*, 1684−1686.

(10) Weber, R. W.; Hoffman, M.; Raine, D. A.; Nelson, H. S. Incidence of bronchoconstriction due to aspirin, azo dyes, non-azo dyes, and preservatives in a population of perennial asthmatics. *J. Allergy Clin. Immunol.* **1979**, *64*, 32−37.

(11) Baptista, M. S.; Indig, G. L. Effect of BSA binding on photophysical and photochemical properties of triarylmethane dyes. *J. Phys. Chem. B* **1998**, *102*, 4678−4688.

(12) Clydesdale, F. M. Color as a factor in food choice. *Crit. Rev. Food Sci. Nutr.* **1993**, *33*, 83−101.

(13) Bolton, J. R.; Bircher, K. G.; Tumas, W.; Tolman, C. A. Figures-of-merit for the technical development and application of advanced oxidation technologies for both electric- and solar-driven systems (IUPAC technical report). *Pure Appl. Chem.* **2001**, *73*, 627−637.

(14) AlHamedi, F. H.; Rauf, M. A.; Ashraf, S. S. Degradation studies of rhodamine B in the presence of UV/H_2O_2. *Desalination* **2009**, *238*, 159−166.

(15) Hameed, B. H.; Lee, T. W. Degradation of malachite green in aqueous solution by Fenton process. *J. Hazard. Mater.* **2009**, *164*, 468−472.

(16) Liang, H.; Zhang, Y.; Huang, S.; Hussain, I. Oxidative degradation of p-chloroaniline by copper oxidate activated persulfate. *Chem. Eng. J.* **2013**, *218*, 384−391.

(17) Soltani, R. D. C.; Safarib, M. Periodate-assisted pulsed sonocatalysis of real textile wastewater in the presence of MgO nanoparticles: Response surface methodological optimization. *Ultrason. Sonochem.* **2016**, *32*, 181−190.

(18) Gemeay, A. H.; El-Ghrabawy, G. R.; Zaki, A. B. Kinetics of the oxidative decolorization of reactive blue-19 by acidic bromate in homogeneous and heterogeneous media. *Dyes Pigm.* **2007**, *73*, 90−97.

(19) Berlin, A. A. Kinetics of radical-chain decomposition of persulfate in aqueous solutions of organic compounds. *Kinet. Catal.* **1986**, *27*, 34−39.

(20) Huang, K.-C.; Zhao, Z.; Hoag, G. E.; Dahmani, A.; Block, P. A. Degradation of volatile organic compounds with thermally activated persulfate oxidation. *Chemosphere* **2005**, *61*, 551−560.

(21) Huang, Y. F.; Huang, Y. H. Identification of produced powerful radicals involved in the mineralization of bisphenol A using a novel UV-$Na_2S_2O_8$/H_2O_2-Fe(II,III) two-stage oxidation Process. *J. Hazard. Mater.* **2009**, *162*, 1211−1216.

(22) Rastogi, A.; Al-Abed, S. R.; Dionysiou, D. D. Sulfate radical-based ferrous-peroxymonosulfate oxidative system for PCBs degradation in aqueous and sediment systems. *Appl. Catal. B* **2009**, *85*, 171−179.
(23) Hussain, I.; Zhang, Y.; Huang, S. Degradation of aniline with zero-valent iron as an activator of persulfate in aqueous solution. *RSC Adv.* **2014**, *4*, 3502−3511.
(24) Khan, Z.; Bashir, O.; Khan, M. N.; Khan, T. A.; Al-Thabaiti, S. A. Cationic surfactant assisted morphology of Ag@Cu, and their catalytic reductive degradation of Rhodamine B. *J. Mol. Liq.* **2017**, *248*, 1096−1108.
(25) Goshisht, M. K.; Moudgil, L.; Khullar, P.; Singh, G.; Kaura, A.; Kumar, H.; Kaur, G.; Bakshi, M. S. Surface Adsorption and Molecular Modeling of Biofunctional Gold Nanoparticles for Systemic Circulation and Biological Sustainability. *ACS Sustainable Chem. Eng.* **2015**, *3*, 3175−3187.
(26) Riedesel, S.; Kaur, R.; Bakshi, M. S. Distinguishing Nanoparticle−Nanoparticle Interactions between Gold and Silver Nanoparticles Controlled by Gemini Surfactants: Stability of Nanocolloids. *J. Phys. Chem. C* **2021**, *125*, 5399−5411.
(27) Kaur, A.; Sandhu, R. K.; Khullar, P.; Singh, K.; Ahluwalia, G. K.; Bakshi, M. S. Colloidal stabilization of sodium dilauraminocystine for selective nanoparticle-nanoparticle interactions: Their screening and extraction by iron oxide magnetic nanoparticles. *Langmuir* **2021**, *37*, 6588−6599.
(28) Pradhan, N.; Pal, A.; Pal, T. Silver nanoparticle catalyzed reduction of aromatic nitro compounds. *Colloids Surf., A* **2002**, *196*, 247−257.
(29) Ghaedi, M.; Biyareh, M. N.; Kokhdan, S. N.; Shamsaldini, S.; Sahraei, R.; Daneshfar, A.; Shahriyar, S. Comparison of the efficiency of palladium and silver nanoparticles loaded on activated carbon and zinc oxide nanorods loaded on activated carbon as new adsorbents for removal of Congo red from aqueous solution: kinetic and isotherm study. *Mater. Sci. Eng.* **2012**, *32*, 725−734.
(30) Marimuthu, S.; Antonisamy, A. J.; Malayandi, S.; Rajendran, K.; Tsai, P.-C.; Pugazhendhi, A.; Ponnusamy, V. K. Silver nanoparticles in dye effluent treatment: A review on synthesis, treatment methods, mechanisms, photocatalytic degradation, toxic effects and mitigation of toxicity. *J. Photochem. Photobiol., B* **2020**, *205*, 111823.
(31) Behnajady, M. A.; Modirshahla, N.; Shokri, M.; Vahid, B. Effect of operational parameters on degradation of malachite green by ultrasonic irradiation. *Ultrason. Sonochem.* **2008**, *15*, 1009−1014.
(32) Rayaroth, M. P.; Aravind, U. K.; Aravindakumar, C. T. Sonochemical degradation of coomassie brilliant blue: Effect of frequency, power density, pH and various additives. *Chemosphere* **2015**, *119*, 848−855.
(33) David, L.; Moldovan, B. Green synthesis of biogenic silver nanoparticles for efficient catalytic removal of harmful organic dyes. *Nanomater* **2020**, *10*, 202.
(34) Saravanakumar, K.; Chelliah, R.; Shanmugam, S.; Varukattu, N. B.; Oh, D.-H.; Kathiresane, K.; Wang, M.-H. Green synthesis and characterization of biologically active nanosilver from seed extract of Gardenia jasminoides Ellis. *J. Photochem. Photobiol., B* **2018**, *185*, 126−135.
(35) Arunachalam, R.; Dhanasingh, S.; Kalimuthu, B.; Uthirappan, M.; Rose, C.; Mandal, A. B. Phytosynthesis of silver nanoparticles using Coccinia grandis leaf extract and its application in the photocatalytic degradation. *Colloids Surf., B* **2012**, *94*, 226−230.
(36) Lueck, H. B.; Rice, B. L.; McHale, J. L. Aggregation of triphenyl-methane dyes in aqueous solution: dimerization and trimerization of crystal violet and ethyl violet. *Spectrochim. Acta* **1992**, *48*, 819−828.
(37) Lewis, L. M.; Indig, G. L. Effect of dye aggregation on triarylmethane-mediated photoinduced damage of hexokinase and DNA. *J. Photochem. Photobiol., B* **2002**, *67*, 139−148.
(38) Petrakova, V.; Sampaio, I. C.; Reich, S. Optical absorption of dye molecules remains unaffected by submonolayer complex formation with metal nanoparticles. *J. Phys. Chem. C* **2019**, *123*, 17498−17504.
(39) Zaheer, Z. Biogenic synthesis, optical, catalytic, and in vitro antimicrobial potential of Ag-nanoparticles prepared using Palm date fruit extract. *J. Photochem. Photobiol., B* **2018**, *178*, 584−592.
(40) Albeladi, A. B.; AL-Thabaiti, S. A.; Khan, Z. Effect of CTAB on the surface resonance plasmon intensity of silver nanoparticles: Stability and oxidative dissolution. *J. Mol. Liq.* **2020**, *302*, 112565.
(41) Henglein, A. Physicochemical properties of small metal particles in solution: "microelectrode" reactions, chemisorption, composite metal particles, and the atom-to-metal transition. *J. Phys. Chem.* **1993**, *97*, 5457−5471.
(42) Darby, B. L.; Auguie, B.; Meyer, M.; Pantoja, A. E.; Ru, E. C. L. Modified optical absorption of molecules on metallic nanoparticles at sub-monolayer coverage. *Nat. Photonics* **2016**, *10*, 40−45.
(43) Wang, P.; Yang, S.; Shan, L.; Niu, R.; Shao, X. Involvements of chloride ion in decolorization of acid orange 7 by activated peroxydisulfate or peroxymonosulfate oxidation. *J. Environ. Sci.* **2011**, *23*, 1799−1807.
(44) Xu, X. R.; Li, X. Z. Degradation of azo dye orange G in aqueous solutions by persulfate with ferrous ion. *Sep. Purif. Technol.* **2010**, *72*, 105−111.
(45) Hayon, E.; Treinin, A.; Wilf, J. Electronic spectra, photochemistry, and autoxidation mechanism of the sulfitebisulfite-pyrosulfite systems. The SO_2^-, SO_3^-, SO_4^-, and SO_5^- radicals. *J. Am. Chem. Soc.* **1972**, *94*, 47−57.
(46) Le, C.; Wu, J.-H.; Li, P.; Wang, X.; Zhu, N.-W.; Wu, P.-X.; Yang, B. Decolorization of anthraquinone dye reactive blue 19 by the combination of persulfate and zero-valent iron. *Water Sci. Technol.* **2011**, *64*, 754−759.
(47) Herrmann, H.; Ervens, B.; Jacobi, H. W.; Wolke, R.; Nowacki, P.; Zellner, R. CAPRAM2.3: a chemical aqueous phase radical mechanism for tropospheric chemistry. *J. Atmos. Chem.* **2000**, *36*, 231−284.
(48) Romero, A.; Santosa, A.; Vicentea, F.; Gonzalezb, C. Diuron abatement using activated persulphate: Effect of pH, Fe(II) and oxidant dosage. *Chem. Eng. J.* **2010**, *162*, 257−265.
(49) Dogliotti, L.; Hayon, E. Flash photolysis of persulfate ions in aqueous solutions. Study of the sulfate and ozonide radical allions. *J. Phys. Chem.* **1967**, *71*, 2511−2516.
(50) Furman, O. S.; Teel, A. L.; Watts, R. J. Mechanism of base activation of persulfate. *Environ. Sci. Technol.* **2010**, *44*, 6423−6428.
(51) Kolthoff, I. M.; Miller, I. K. The chemistry of persulfate. I. The kinetics and mechanism of the decomposition of the persulfate ion in aqueous medium. *J. Am. Chem. Soc.* **1951**, *73*, 3055−3059.
(52) Huang, D.; Chen, N.; Zhu, C.; Fang, G.; Zhou, D. The overlooked oxidative dissolution of silver sulfide nanoparticles by thermal activation of persulfate: Processes, mechanisms, and influencing factors. *Sci. Total Environ.* **2021**, *760*, 144504.
(53) Park, C. M.; Heo, J.; Wang, D.; Su, C.; Yoon, Y. Heterogeneous activation of persulfate by reduced graphene oxide−elemental silver/magnetite nanohybrids for the oxidative degradation of pharmaceuticals and endocrine disrupting compounds in water. *Appl. Catal., B* **2018**, *225*, 91−99.
(54) Wilmarth, W. K.; Haim, A. In *Peroxide Reaction Mechanisms*; Edwards, J. O., Ed.; John Wiley & Sons: New York, 1962; pp. 175−225.
(55) Liang, C.; Su, H. Identification of sulfate and hydroxyl radicals in thermally activated persulfate. *Ind. Eng. Chem. Res.* **2009**, *48*, 5558−5562.
(56) Aninipsitakis, G. P.; Dionysiou, D. D. Radical generation by the interaction of transition metals with common oxidants. *Environ. Sci. Technol.* **2004**, *38*, 3705−3712.
(57) Li, G.; Wong, K. H.; Zhang, X.; Hu, C.; Yu, J. C.; Chan, R. C. Y.; Wong, P. K. Degradation of acid orange 7 using magnetic AgBr under visible light: the roles of oxidizing species. *Chemosphere* **2009**, *76*, 1185−1191.
(58) Buxton, G. V.; Greenstock, C. L.; Helman, W. P.; Ross, A. B. Critical review of rate constants for reactions of hydrated electrons, hydrogen atoms and hydroxyl radicals ($^{\cdot}OH/^{\cdot}O^-$) in aqueous solution. *J. Phys. Chem. Ref. Data* **1988**, *17*, 513−886.

https://doi.org/10.1021/acsomega.1c04501
ACS Omega 2021, 6, 27510−27526

(59) Al-Asfar, A.; Zaheer, Z.; Aazam, E. S. Eco-friendly green synthesis of Ag@Fe bimetallic nanoparticles: Antioxidant, antimicrobial and photocatalytic degradation of bromothymol blue. *J. Photochem. Photobiol., B* **2018**, *185*, 143−152.
(60) Colonna, G. M.; Caronna, T.; Marcandalli, B. Oxidative degradation of dyes by ultraviolet radiation in the presence of hydrogen peroxide. *Dyes Pigm.* **1999**, *41*, 211−220.
(61) Aleboyeh, A.; Olya, M. E.; Aleboyeh, H. Electrical energy determination for an azo dye decolorization and mineralization by UV/H_2O_2 advanced oxidation process. *Chem. Eng. J.* **2008**, *137*, 518−524.
(62) Gosetti, F.; Gianotti, V.; Angioi, S.; Polati, S.; Marengo, E.; Gennaro, M. C. Oxidative degradation of food dye E133 brilliant Blue FCF liquid chromatography−electrospray mass spectrometry identification of the degradation pathway. *J. Chromatogr. A* **2004**, *1054*, 379−387.
(63) Khan, M. N.; Bashir, O.; Khan, T. A.; AL-Thabaiti, S. A.; Khan, Z. CTAB capped synthesis of bio-conjugated silver nanoparticles and their enhanced catalytic activities. *J. Mol. Liq.* **2018**, *258*, 133−141.
(64) Yousefi, M.; Ghanbari, F.; Zazouli, M. A.; Madihi-Bidgoli, S. Brilliant Blue FCF degradation by persulfate/zero valent iron: The effects of influencing parameters and anions. *Desalin. Water Treat.* **2017**, *70*, 364−371.
(65) Shahmoradi, B.; Malekia, A.; Byrappa, K. Photocatalytic degradation of Amaranth and Brilliant Blue FCF dyes using in situ modified tungsten doped TiO_2 hybrid nanoparticles. *Catal. Sci. Technol.* **2011**, *1*, 1216−1223.
(66) Rauf, M. A.; Ashraf, S.; Alhadrami, S. N. Photolytic oxidation of Coomassie Brilliant Blue with H_2O_2. *Dyes Pigm.* **2005**, *66*, 197−200.
(67) Scott, R.; Mudimbi, P.; Miller, M. E.; Magnuson, M.; Willison, S.; Phillips, R.; Harper, W. F. Advanced Oxidation of Tartrazine and Brilliant Blue with Pulsed Ultraviolet Light Emitting Diodes. *Water Environ. Res.* **2017**, *89*, 24−31.
(68) Bakshi, M. S.; Possmayer, F.; Petersen, N. O. Aqueous phase room temperature synthesis of gold nanoribbons: Soft template effect of a gemini surfactant. *J. Phys. Chem. C* **2008**, *112*, 8259−8265.
(69) Pouretedal, H. R.; Keshavarz, M. H. Synthesis and characterizationof Zn1−XCuXS and Zn1 − XNiXS nanoparticles and their applications as photocatalyst in Congo red degradation. *J. Alloys Compd.* **2010**, *501*, 130−135.

https://doi.org/10.1021/acsomega.1c04501
ACS Omega 2021, 6, 27510−27526